

**A STUDY ON THE RESPONSE OF HUMAN PHANTOM
AORTA TO EXTERNALLY IMPOSED OSCILLATIONS**

Yusuf Liyakat Khan

Master of Philosophy

2018

A STUDY ON THE RESPONSE OF HUMAN PHANTOM AORTA TO EXTERNALLY IMPOSED OSCILLATIONS

Primary Supervisor: Dr. Andrew Lowe

Secondary Supervisor: Prof. Ahmed Al-Jumaily

A thesis submitted to Auckland University of Technology in
fulfilment of the requirements for the degree of Master of
Philosophy

June 2018

School of Engineering

Faculty of Design and Creative Technologies

Institute of Biotechnology (IBTec)

Abstract

This study of forced oscillation effects on phantom human aorta is a concept extended from previous research on airway smooth muscle to a study of aortic tissue, and the phenomena that induce oscillations in the aorta modelled as a fluid-conveying pipe. The study was carried out to measure the pressures and flows at different frequencies and amplitudes with material properties, the pulsatile nature of blood flow as distinct from respiration, and differing boundary conditions. Mathematical modelling, software simulation and experimental work on human phantom aorta were carried out.

The simulation was done using Wolfram (Mathematica[®]10, USA) software. The 1-Dimension mathematical model for pressure and velocity was simulated for different signals and boundary conditions. The simulation was fitted with interpolation and to produce one beat with all the information to be repeated. The simulation response was compared with the experimental set up.

The experimental set up, using the phantom human aorta, was used to verify the simulation responses. Dragon Skin[®]10 was used as material to make the phantom aorta. The phantom aorta was submerged in fluid (water) to give boundary conditions more similar to a human aorta for the readings. The readings used a function generator, LDS[®] V406 shakers along with LDS[®] PA 100E power amplifier and force displacement transducer to get output responses. The readings were taken from frequencies between 5 Hz to 49 Hz with 1-2 Vpp amplitude. The response to the forced oscillations were significant for the frequency range between 30 Hz and 35 Hz with maximum amplitude of 2 Vpp in excitation magnitude. However, the ascending aorta showed reduced values under the same conditions. In contrast, flow had a very weak response between 5 Hz to 20 Hz; only at higher frequencies flow did more vibrations occur which made the experimental set up unstable.

Contents

Abstract	3
List of figures	6
List of Tables.....	9
Glossary/Abbreviations.....	10
Symbols of Equations with units	11
Attestation of Authorship	12
Acknowledgement.....	13
Chapter 1: Introduction.....	14
1.0 Background	14
1.1 Overview of the Cardiovascular System.....	14
1.2 Aorta	16
1.2.1 The Systemic Circulation of the Major Arteries.....	16
1.2.2 The Branches of the Abdominal Aorta.....	18
1.2.3 Arterial pressure waveform during a cardiac cycle	18
Chapter 2: Literature Review.....	20
2.0 Introduction	20
2.1 Physical model of the arterial system.....	21
2.1.1 Arterial Tree Modelling	21
2.1.2 Comparison of Windkessel, 1-D, 3-D models for Pulse Wave Propagation	21
2.1.3 Comparison of 1D and 2D Arterial Models.....	22
2.1.4 One dimensional equation (1D) [38]	23
2.2 1D Models	23
2.2.1 Multibranched human arterial model	23
2.2.2 Individual Tube models.....	25
2.2.3 Windkessel models and functional arterial parameters: stiffness and resistance	26
2.3 Cardiovascular System Biomechanics	28
2.4 Recent Work on Active Forces at AUT	29
2.5 Objectives	30
2.5 Thesis Structure	30
Chapter 3: Theory and Simulation	31
3.1 Introduction	31
3.2 Mathematical Model.....	31
3.3 Methodology - Simulation Model	33

3.3.1 Model Geometry	33
3.3.2 Different Simulation Scenarios.....	34
3.4 Results.....	35
Chapter 4: Experimental Analysis	38
4.1 Introduction	38
4.2 Aim.....	38
4.3 Methodology.....	38
4.3.1 The Phantom Aorta	38
4.3.4 Aorta Phantom Experimental Simulation Setup	39
4.4 Modifications to introduce mechanical displacements.....	44
4.4 Results.....	49
4.5 Results from the final cardiovascular simulation setup	57
Chapter 5: Discussion on the Analysis of the Simulation and Experimentation results	63
5.1 Introduction	63
5.2 Discussion of Simulation and Experimental results	63
5.3 Final comments	68
Chapter 6: Conclusion and future scope	69
6.1 Conclusion	69
6.2 Future Scope	70
Appendix A: Simulation Coding of Mathematica for mathematical model.....	71
Appendix B: Smart Motor programming code.....	73
Appendix C: LDS Shaker 405 and LDS® PA 100E power amplifier	74
Appendix D: Dragon Skin® 10 Specifications	79
Appendix E: Easy Driver Schematic V1.1.....	80
References	81

List of figures

Figure 1.1: Overview of the human cardiovascular system [1].....	14
Figure 1.2: Cardiovascular system of Human [3].....	16
Figure 1.3: Arterial Pressure waveform during a cardiac cycle [7].....	18
Figure 2: Windkessel effect of elastic and rigid element: (a) Pressure (b) Amplitude [29].....	26
Figure 2.1: Thesis structure.....	29
Figure 3.1: Transient flow through a pipe.....	30
Figure 3.2: Phantom Aorta [56].....	32
Figure 3.3: Model 1 Sinewave – Pressure.....	34
Figure 3.4: Model 1 Sinewave – Flow.....	34
Figure 3.5: Impulse signal.....	35
Figure 3.6: Model without beat.....	35
Figure 3.7: Final Model with beat and interpolation.....	35
Figure 3.8: Interpolation fitting.....	36
Figure 3.9: Beat signal.....	36
Figure 4.1: Johnson’s phantom aorta shape [56-58].....	38
Figure 4.2: (A1): Reservoir 1. (A2) Reservoir 2. (B): Bellow system. (C): Valves. (D): Phantom aorta 2. (E): Linear actuator. (F): Capillaries [56]	39
Figure 4.3: (A): piGrip [®] bellows uncompressed. (B): piGrip [®] bellows compressed [56].....	39
Figure 4.4: (A): 3D printed bush. (B): 3D printed frame for the piGrip [®] bellows [56]	40
Figure 4.5: The piGrip [®] bellows along with coupling and bush [56]	40
Figure 4.6: The reservoirs of 12 mm diameter hose connections.....	41
Figure 4.7: (A): Brass check valve. (B): PVC piping. (C): Bellow system. (D): Aortic valve [56].....	41
Figure 4.8: Prosthetic aortic valve (CardiaMed Rotating Heart Valve) supplied by OBEX [®]	42
Figure 4.9: Artificial capillary system (A): 12 mm push fitting (B): PVC pipe (C): Cylindrical Sponge [56].....	42
Figure 4.10: Camming profile was uploaded to the SmartMotor [56]	43

Figure 4.11(a): Initial Modified experimental setup: (A) Phantom Aorta. (B) Transonic Flow meter. (C) Amplifier. (D) SmartMotor™	44
Figure 4.11(b): Initial Modified experimental setup: (E) LDS® V406 shakers.....	44
Figure 4.12: LDS® V406 shakers.....	44
Figure 4.13: Initial modified schematic block diagram of cardiovascular simulation setup.....	45
Figure 4.14: Aorta submerged in the fluid.....	47
Figure 4.15: (A) Force displacement Transducer. (B) Clamp holding.....	48
Figure 4.16: LabChart Normal (without any forced oscillations.....	49
Figure 4.17: LabChart for Sinewave of 10Hz and 1Vpp amplitude forced oscillation direct from function generator.....	49
Figure 4.18: Channel A measurement Spectrum of Ascending Aorta (AO) at 5Hz and 1Vpp.	50
Figure 4.19: Channel A and B, Spectrum of Ascending Aorta (AO) Descending Aorta (DA) at 5Hz and 1Vpp.....	51
Figure 4.20: Comparison of Spectra at Channel A for Pressure wave.....	52
Figure 4.21: Comparison of Spectra at Channel B for Pressure wave.....	52
Figure 4.22: Flow Measurement Channel A.....	53
Figure 4.23: Comparisons of Flow Measurement Channel A.....	53
Figure 4.24: Comparison Flow Measurement Channel B.....	54
Figure 4.25: Higher Frequencies Pressure Measurement Channel A.....	54
Figure 4.26: Comparison of Channel A and B for Ascending aorta (AO) and Descending Aorta (DA) Pressures.....	55
Figure 4.27: Comparison of Pressure Spectra at Channel A	55
Figure 4.28: Comparison of Pressure Spectra at Channel B.....	56
Figure 4.29: Comparison of pressure gain spectral at different voltages.....	58

Figure 4.30: Comparison of pressure gain spectral at different frequencies.....	58
Figure 4.31: Comparison of pressure gain spectral at different locations.....	59
Figure 4.32: New Experimental Setup Normal Spectrum of Pressure- Descending Aorta (Phantom) without forced oscillation.....	59
Figure 4.33: Comparison of flow gain spectral at different voltages.....	60
Figure 4.34: Comparison of flow gain spectral at different frequencies.....	60
Figure 4.35: Comparison of flow gain spectral at different locations.....	61

List of Tables

Table 3.1: Initial test simulation model geometry of phantom aorta [56].....	32
Table 3.2: Comparisons of all the scenarios with their applied signals.....	33
Table 4.1: Dimensions of the aorta [56-58].....	38
Table 4.2: Measurement equipment used for cardiovascular simulation set up.....	46
Table 4.3: Pressure Descending (DA) and Ascending Aorta (AO).....	57
Table 4.4: Flow Descending (DA) and Ascending Aorta (AO).....	57
Table 5.1: Descending Aorta Pressure output from 30 Hz to 35 Hz under different amplitudes.....	63
Table 5.2: Comparisons of DA and AO Pressure output from 30 Hz to 35 Hz.....	64
Table 5.3: Comparison of Descending and Ascending Aorta Flow measurement.....	66

Glossary/Abbreviations

Aorta:

A major Artery of human being that supplies blood to every parts of the body

Arteries:

It emerges from the main artery, they are tubular muscular walled forms the network in the circulation system in which blood is flowing

Ascending Aorta (AO):

Emerge as the top part of aorta near to the heart

BVP = Boundary Value Problems

Cardiac output:

The amount of blood pumped out of the heart per minute. Expressed in L/min usually

Descending Aorta (DA):

It is the bottom part of aorta that moves away from the heart

ET = Arterial stiffness

Haemodynamic:

Flowing of blood in the tissues and organs

Pb = Pressure backward of blood

Pd = Pressure diastolic of blood

Pf = Pressure forward of blood

PP = Pulse Pressure of blood

Phantom Aorta:

An artificial part of the human cardiovascular system

Pulse Wave Velocity (PWV):

Arterial stiffness measurement, or the rate of pressure wave moving down in blood vessel

Veins:

It carries the deoxygenated blood to the heart

Zc = Characteristic Impedance

Symbols of Equations

SI units are given, with common alternatives where applicable

A = area, m^2

c = wave speed, m/s

ρ = density of fluid, kg/m^3

D = diameter of aorta, m

E = modulus of elasticity, Pa

g = acceleration due to gravity, m/s^2

H = Pressure head, m

h = height of aorta, m

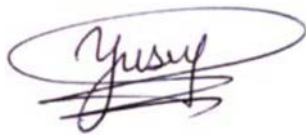
P = aorta pressure, Pa or mmHg

Q = flow discharge, m^3/s or L/min

x = distance of pipe, m

Attestation of Authorship

I hereby declare that this thesis submission is a record of my original work produced from the best of my ideas and knowledge. It contains no material previously published or written by another person (except where explicitly defined in the acknowledgements) nor material which to a substantial extent has been submitted for the award of any other degree or diploma of a university or other institution of higher learning.

A handwritten signature in purple ink, appearing to read 'Yusuf', is enclosed within a light purple oval. Below the signature is a solid black horizontal line.

Yusuf Liyakat Khan

18 October 2018

Acknowledgement

I give my sincere thanks to Almighty God to keep me agile and help to focus for the completion this task in the service of humanity.

My deep and sincere gratitude to my primary supervisor **Dr. Andrew Lowe** for giving me constant light of guidance with his knowledge, patience, motivation and great insight of this research process in my entire journey of learning for this Master of Philosophy thesis. I am thankful to my secondary supervisor **Prof. Ahmed Al-Jumaily** for his encouragement and timely valuable advice for this research work.

I would like to thank the Institute of Biomedical Technologies of AUT, staff and students who directly or indirectly helped in my journey of learning. I would like to acknowledge the following important people:

Parn Jones, ME (AUT, for his sincere help in experimental set up)

Barbara Morris, MEd (Hons), (Western Institute of Technology at Taranaki (WITT) for providing her support in very short time for proof reading of my thesis)

Dr. Saghir Ahmed, PhD (Massey University for motivation)

My mother for her blessings and prayers. My brother and sister who have supported me to keep my morale high in this journey.

Chapter 1: Introduction

1.0 Background

The heart is the most vital organ of the human body, it plays a very important role in transporting the blood to every part of the body. The heart pumps oxygenated blood from the lungs to the heart and then to various parts of the body through arteries. It carries de-oxygenated blood from various parts to the lungs passing through the heart, through the veins.

In order to study the arterial responses to the external forced oscillations, a force can be applied to the descending part of the aorta. The aorta is the major systemic artery which ascend from the heart and then descends into various arteries. The present research will give an insight about the responses of the aorta to applied forced oscillations at descending aorta by observing output responses at both descending and ascending aorta.

The motivation behind the aim of this project is to investigate how superimposed oscillations phenomena for lung relaxation may also possibly be used in the cardiovascular system for managing blood pressure through induced responses in the aorta. Two such phenomena are forces arising due to fluid momentum and forces arising due to whole body vibrations. An analytical model and simulation will be used to inform an experimental (in-vitro) investigation in simulation aortic tissue.

1.1 Overview of the Cardiovascular System

The circulatory system consists of the following;

- Arteries
- Arterioles
- Capillaries
- Venules
- Veins

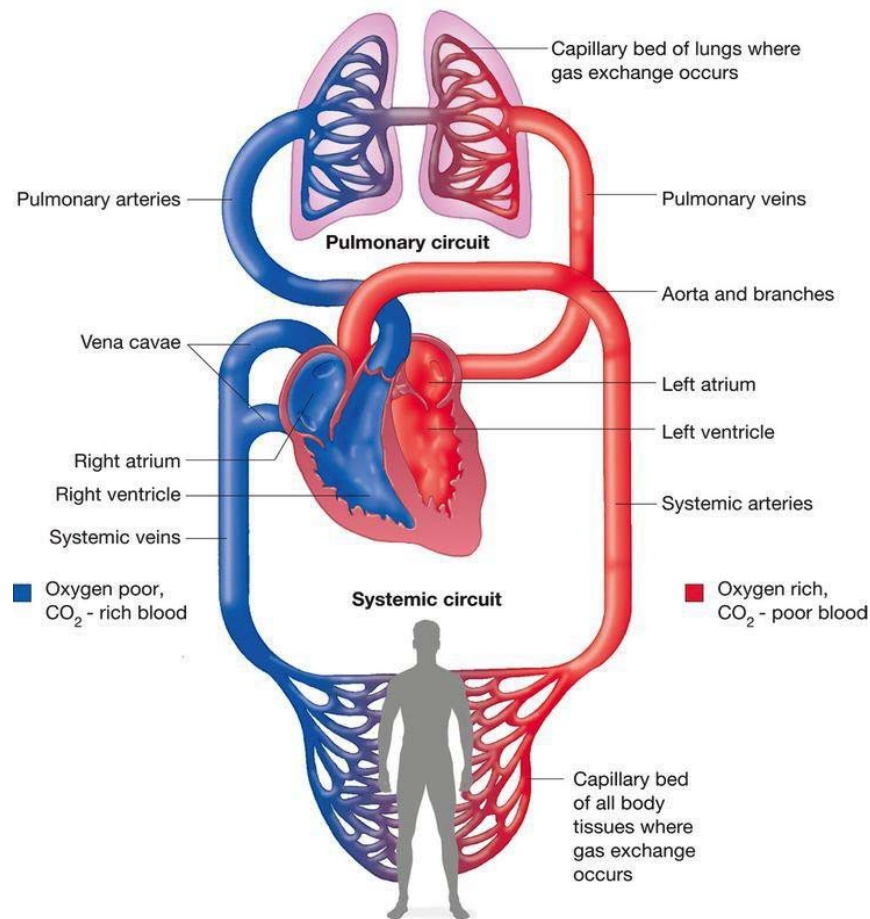


Figure 1.1: Overview of the human cardiovascular system [1].

The blood circulatory system is known as the cardiovascular system (Figure 1.1). The entire cardiovascular system consists of heart, blood and blood vessels. The aorta is known as the primary artery and the main function of the aorta is to distribute the oxygenated blood to the body to maintain the blood pressure [2]. Branches from the aorta supply blood to every vital organ in the human body. The venous system brings back the deoxygenated blood to the heart. The circulatory system also transports oxygen and carbon dioxide absorbed products of digestion and metabolic waste to liver and kidneys along with immune cells, hormones, clotting proteins, and through the regulation of skin blood flow, performs thermoregulation.

There are many abnormalities and diseases that have an impact on the cardiovascular system which are called cardiovascular diseases. The diseases that arise from the cardiovascular system are mainly two types firstly, congenital diseases present at the birth and the other due to lifestyle or daily habits, such as lack of physical activity and drinking, smoking and over eating. The common symptoms associated with these diseases are high blood pressure or low blood pressure

in some cases. This results in higher probability of aneurysm and risk of stroke. At present these diseases are normally treated by using oral medication or surgery.

1.2 Aorta

1.2.1 The Systemic Circulation of the Major Arteries

The largest artery of the body is aorta. The aorta in adults is about 2-3 cm in diameter (about 1 in.) and it starts from the left ventricle of the heart. The diameter decreases as it descends to its terminal position in various organs. The aorta's branches are named based on their shape or location. The aorta goes slightly upward from the left ventricle of the heart, it is called the ascending aorta, and has arches to the left side called the aortic arch. It goes downward, via thorax, passing the spine (thoracic aorta) and enters the diaphragm and then into the abdominopelvic cavity where it is known as the abdominal aorta (figure 1.2). The Aortic Arch is about 4-5 cm (almost 2 inches) and it has the following branches which are namely, the brachiocephalic trunk which is the first branch that splits into the right common carotid and right artery [3]. The second branch from the aortic arch is the left common carotid artery which further divides into left internal carotid artery which goes to the brain and the left external carotid. It further goes to the muscles and skin of neck and head. The third branch goes from the aortic arch, which is the left subclavian artery, then goes to the vertebral artery to serve the few parts of the brain. The subclavian artery forms the axillary artery which further continues to become the brachial artery to supply the blood to the arms. It further divides into radial and ulnar arteries at the elbow to supply blood to forearm.

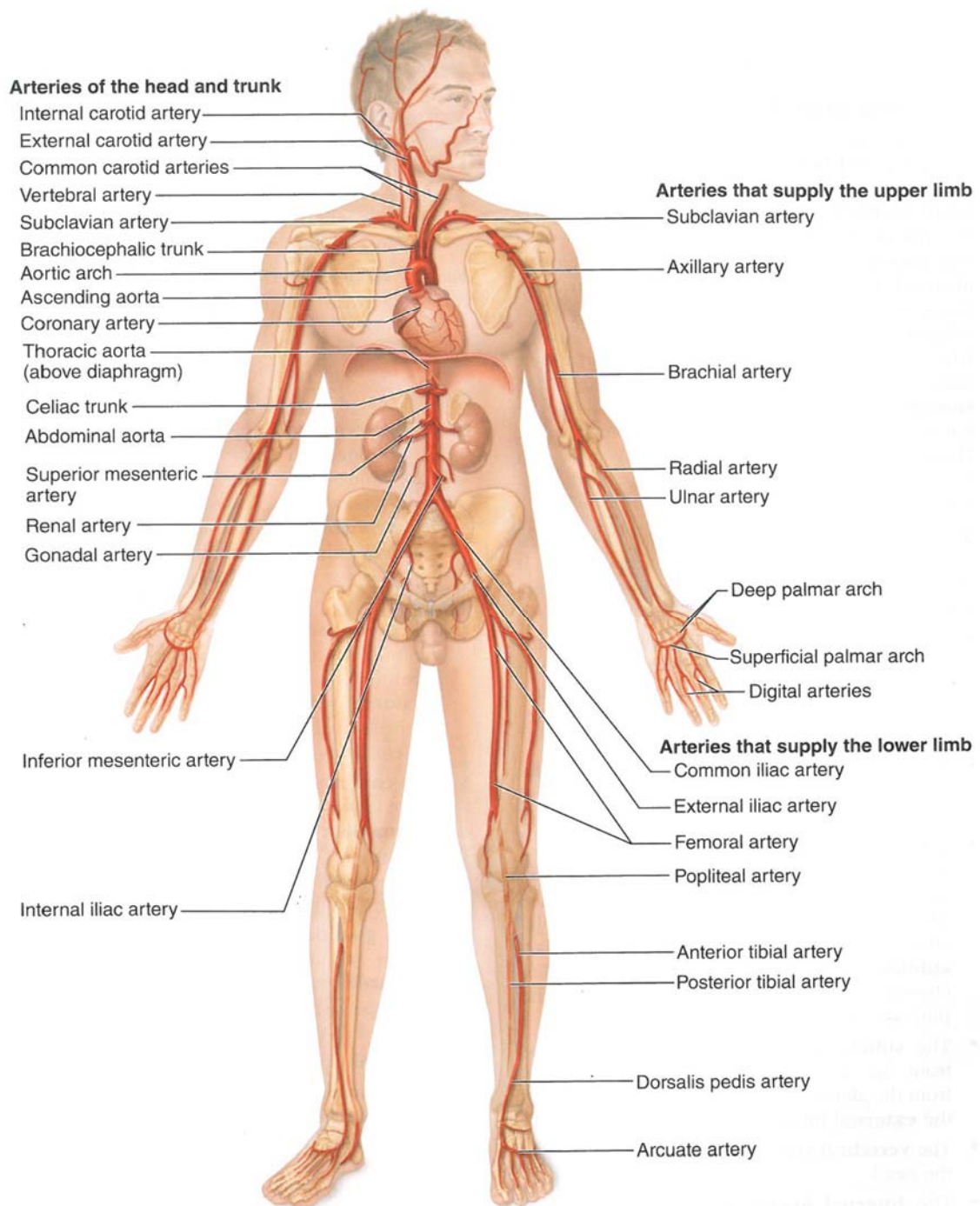


Figure 1.2: Cardiovascular system of Human [3]

The thoracic aorta branches to form the intercostal arteries in 10 pairs to serve the thorax wall muscles, while the other branches the thoracic aorta serves are the bronchial arteries of the lungs, oesophageal arteries of the oesophagus and phrenic arteries of the diaphragm.

1.2.2 The Branches of the Abdominal Aorta

The first branch of the abdominal aorta is called the celiac trunk. This is a single vessel which has 3 branches namely; 1. Left gastric artery, to serve the stomach 2. Splenic artery, serve the spleen; and 3. Hepatic artery, to serve the liver.

According to Fiore and Schmidt [4], due to the elastic nature of the walls of aorta, the blood pressure is maintained in the entire human body. When the aorta receives the blood from the heart it recoils to the pulsating blood pressure which is transported to whole body by the capillaries, although the pressure oscillation decreases due to the branching of the capillaries.

The Aorta is histologically formed by mixtures of endothelial cells, smooth muscle cells, nerves, extracellular matrix and the likeness of fibroblast cells. The aorta is lined by chemoreceptors and baroreceptors which act as a relay to carry information about the requisite levels of the blood pressure, carbon dioxide and blood pH levels to the brain.

In summary, the aorta is a highly complex and specialised part of the cardiovascular system for transporting the oxygenated blood to the whole body and not just an ordinary tube. The main function is to carry blood away from the left ventricle [5]. It also helps with arterial and myocardial perfusion functions for the whole cardiovascular system [6]. The elastic nature of aorta induces pulses which propagate in the entire aorta in response to blood flow and to maintain the blood pressure in the body. Normal blood pressure and normal blood flow is maintained due to the vital role played by the elastic nature of aortic walls.

1.2.3 Arterial pressure waveform during a cardiac cycle

When blood is pumped or ejected into the aorta from the left ventricle, during which the elastic walls of the aorta are stretched due to this, the aortic pressure is marginally below ventricular pressure during the time of ejection. The elastic recoil of the aorta is due to the drop in the pressure in the ventricle below the pressure in the aorta. This results in blood flow toward the ventricle. Subsequently, the aortic valve closes and due to this, the pressure in the aorta increases slightly. This gives a dicrotic notch in the pressure of the aorta (refer

to figure 1.3). The meaning of dicrotic is “double-beating”, whenever there is an increase in the pressure because of recoil a double pulse can be felt. The other name for the dicrotic notch is “incisura” which means a cutting into. The pressure in the aorta starts gradually falling during ventricular diastole as blood flows through the peripheral vessels. After the aortic pressure reaches approximately 80 mm Hg the ventricle contracts to force once again more blood into the aorta. In clinical studies the blood pressure changes in the aorta are considered rather than in the left ventricles for blood pressure measurement. For a young adult who is at rest, blood pressure in the aorta fluctuates between 120 mm Hg systolic and 80 mm Hg diastolic.

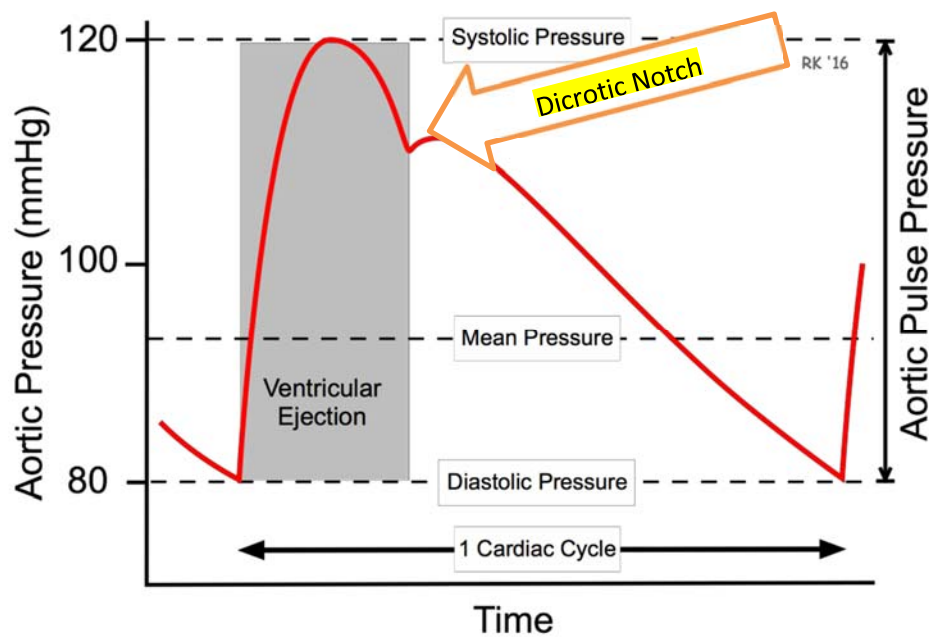


Figure 1.3: Arterial Pressure waveform during a cardiac cycle [7].

Chapter 2: Literature Review

2.0 Introduction

The aorta is the largest artery in the body, rising from the heart's major pumping chamber, the left ventricle. The walls of the aorta are made up of three different layers of tissue: a thin inner layer (intima); a thick, elastic middle layer (media); and a thin outer layer (adventitia). The structure of these layers is important to the proper functioning of the aorta [8]. In the normal aorta, the elastic fibres are present throughout and are especially dense in the wall of the ascending aorta, which experiences the greatest force with each heartbeat. These components are normally under tension as indicated by the contraction of the vessel length and diameter. Moreover, excessive aortic vibrations may also be a major cause of fatigue failure [9-10]. Excessive aortic vibrations levels usually occur when a mechanical natural frequency of the aortic system is excited by some pulsation or mechanical source. The vibration mode shapes usually involve lateral vibrations and/or shell wall radial vibrations [11-17]. Although an analogy with industrial systems has been studied previously in the biomedical literature [18-22], the study and the understanding of the dynamics of this branch is rather complicated due to the coupling effects and due to the heterogeneity of the organ radially [8] as well as other factors. There is a major need for practical as well as scientific information on the behaviour of the aortic wall under different kinds of oscillations.

In previous work performed by the Institute of Biomedical Technologies (IBTec), Auckland University of Technology [23-25], it has been found that the active force in contracted airway smooth muscle is reduced by imposition of vibrations (tidal and length oscillations) and that these interactions are dependent on both frequency and duration. Although the structure of the aorta is different to lung tissue, there are similarities, including both trachea and aorta having multi-unit smooth muscle media layers.

This work will extend the IBTec research on airway smooth muscle to a study of aortic phantoms, and the phenomena that induced oscillations in the aorta modelled as a fluid-conveying pipe. Particular differences will be the different material properties, the pulsatile nature of blood flow as distinct from respiration, and differing boundary conditions.

2.1 Physical model of the arterial system

2.1.1 Arterial Tree Modelling

The advancement in vascular flow simulation methods for large arterial trees gives our present research an important perspective on blood flow simulation which is one of the vital parts of the research under this study. There are two types of methods considered according to the vessel diameter such as;

According to Anor et al. [37], “

(a) Macrovascular Network (MaN), which includes large arteries down to a diameter of 0.5 mm.

(b) Mesovascular Network (MeN), which consists of small arteries and arterioles, varying from 500 μm down to 10 μm by forming a tree like structure.

(c) The Microvascular Network (MiN), which represents the capillary bed, following a mesh-like structure”. In consideration of Anor et al. [37], we conclude that it gives more confidence in the present research to develop a mathematical model for simulation and subsequent use for validation with an experimental set up. Although in other work simulations were done for large arterial networks, such as the intracranial tree, this makes our research easier as we are dealing with only one major artery of cardiovascular system i.e. aorta.

However, it also demonstrates that new multiscale modelling methods are required for understanding the effects of complex multiscale pathophysiological processes which is part of cardiovascular diseases [37]. At present, typical 3D simulation of blood vessels requires several days of computation. To reduce time, optimization is required primarily for the two most difficult time-consuming steps, being construction of anatomical geometry and numerical calculations. The main that question remains is, do the proposed methods offer clinical value? Our research is confined to the artificial set up at present, with an emphasis on simulation results which can be validated in future, while an actual human aorta will have more clinical value.

2.1.2 Comparison of Windkessel, 1-D, 3-D models for Pulse Wave Propagation

The physical and mathematical modelling of pulse wave propagation is based on general fluid dynamical principles. Modelling may cover adaptation of the arterial system over short and long

terms and must deal with uncertainties in personalised model parameters and boundary conditions. The main methodologies used are as follows;

- (a) Windkessel models: This model provides a lumped description without permitting studies of pressure and flow wave propagation. It has got limited parameters which represent the main properties of the arterial tree distal to the point of interest [47].
- (b) 1-D models or Distributed models: They are formed by breaking up the major arterial tree into minor segments with known mechanical properties and geometry. Womersley's (1957) oscillatory flow theory shows characteristics of wave transmission. Arterial tree models can also be made based on 1D Navier-Stokes equation for mass and momentum conservation. For transmission of local pressure and flow models, 1D is very useful and the same has been used in our mathematical model simulation [47].
- (c) 3-D models: These are usually for the detailed information. The 3D model is needed in predicting complex fluid phenomena for specific flow in the arterial site with realistic boundary conditions. There is rigorous use of Computational Fluid Dynamics (CFD) for 3D models [47].

Numerous aspects of circulatory, physiology and pathology are dictated by the pulsatile nature of blood flow. The true physical quantities and right parameters will yield pressure and flow predictions accurately by 1D model [47]. There is a limitation to microcirculation models based on linear Windkessel models which do not model reflection *in vivo* during autoregulation which involves neurovascular coupling as described in Martens et al.(2009) [48]. Ideally, models will also be amenable to experimental measurement for sensitivity analysis. Arterial models should also be coupled with the venous system, which requires appropriate modelling and taking into account the particularities of venous and cerebrospinal flow (e.g., valves and collapsible tubes) [47]. However, the present research is limited to the 1-D and limited to only aorta and no other arteries and veins.

2.1.3 Comparison of 1D and 2D Arterial Models

The arterial model is easily solvable analytically with both a one dimensional (1D) and also with a two dimensional (2D) model. There have been various models: Linear and non-linear in one dimensional and two dimensional models. All models are useful to understand the arterial tree [38].

Due to conceptual understanding of vessel response there is no exact model that can represent all arterial properties. A useful model generates waveforms free from artefacts.

The choice of model is based on its degree of complexity and schemes of computational solutions.

2.1.4 One dimensional equation (1D) [38]

Important assumptions made about the vessel are that it is elastic, isolated and circular, these are our considerations for our simulation mathematical model with variable circular tube with tapering in length. Blood was considered as Newtonian and incompressible fluid flowing in the vessel according to Navier-Stoke equation. Therefore equation 1 is given on basis of the continuity and equation 2 is based on the momentum of fluid dynamics [38].

$$\frac{\partial A}{\partial t} + \frac{\partial(uA)}{\partial x} = 0 \text{ ----- (1)}$$

$$\frac{\partial u}{\partial t} + u \frac{\partial u}{\partial x} + \frac{1}{\rho} \frac{\partial P}{\partial x} = - \frac{8\pi\mu u}{\rho A} \text{ ----- (2)}$$

Two dimensional equation [38]:

$$\frac{\partial u}{\partial t} + u \frac{\partial u}{\partial x} + v \frac{\partial u}{\partial r} + \frac{1}{\rho} \frac{\partial P}{\partial x} = \vartheta \left(\frac{\partial^2 u}{\partial x^2} + \frac{1}{r} \frac{\partial u}{\partial r} + \frac{\partial^2 u}{\partial r^2} \right) \text{ ----- (3)}$$

$$\frac{\partial u}{\partial t} + 2(1 - \alpha) \frac{u}{r} \frac{\partial r}{\partial t} + \alpha u \frac{\partial u}{\partial x} + \frac{1}{\rho} \frac{\partial P}{\partial x} = \frac{-2\vartheta\alpha u}{\alpha - 1r^2} \text{ ----- (4)}$$

By using eqn. 2 and eqn. 4 we can develop an empirical relationship between pressure and radius. This is very important for the present research simulation model development [38].

$$A = \pi(R_0 + \beta p)^2 \text{ ----- (5)}$$

A denotes cross sectional area, u axial blood velocity, x the axial coordinate, R_0 is vessel radius at zero pressure, and β is the compliance constant of the vessel. The present research starts with 1D equations. In consideration of Ohgre et al. [38], we conclude that the 1D equation is easier to compute and can easily be analysed, although it gives the same results as 2D equations.

2.2 1D Models

2.2.1 Multibranched human arterial model

Avolio's [41] model incorporates the origin of reflected pressure waves in arterial system of a human multi-branched arterial tree. The model represents the human arterial tree architecture

which encompasses physical properties and bifurcation of the arterial segments. This model uses spectral techniques on pressure and flow waves along with linear theory [41]. The model does not include the nonlinear elastic properties of arteries [41]. It found that the most profound changes in the systemic input impedance occur due to alteration in reflection coefficients of vascular beds [42]. It calculates impedance of the ascending aorta which is in close agreement with previous publications. It has introduced pressure wave propagation mapping techniques. The aorta behaves differently in periphery in terms of retrograde transmission. In consideration of Karamanoglu et al. [42], we conclude that there are a few shortcomings - it does not include nonlinear elastic properties of the arteries and also the tapering of arterial segments is not included. However, the present research does incorporate a changing diameter of the aorta.

1-D model of blood flow in compliant vessels to study the effect of local stiffening of an artery on the flow and wave propagation patterns is a very important aspect for the present research which gives the numerical investigation of a 1-D model of blood flow in human arteries using Galerkin and a Taylor–Galerkin formulation. The methodology of using the Governing Equations, Discontinuous Galerkin Method, and Taylor–Galerkin Method with adoption of simplified model consisting of the 55 main arteries in the model was used by Sherwin et al. [28]. They showed that the terminal resistance generates regions of reversed flow and also produces a waveform in the ascending aorta which includes a dicrotic notch. This gives us an important basis of our research to apply forced oscillations at descending aorta and see the effects on ascending aorta [28]. The dicrotic notch is a physiological feature that has been observed in flow measurements in vivo. Sherwin et al. leave an unanswered question about how to model reflected waves at the bifurcations and these reflections lead to superimposition of waves which might result in increased peak pressures at other points of the arterial tree [28].

Specifying the outlet flow conditions is needed in 3D incompressible flow simulation within a rigid geometry. The proper outlet flow conditions in blood flow simulations through asymmetric arterial bifurcations were investigated by prototyping asymmetric arterial bifurcation and are modified by developing the daughter vessels to mimic effects of stenosis [33].

The boundary conditions of the 3D simulations have been implemented on commercial software, FLUENTTM for the outflow boundary conditions. 1D outlet conditions are effectively implemented to produce a full time-dependent model [33]. The concept of using 1D outlet conditions with 3D simulation is very noteworthy for the present research which has the simulation of 1D mathematical equations. In considering Johnson et al. [33], we conclude that it

has shortcomings in that it does not investigate 3D geometry (like curvature), blood properties (like viscoelasticity), and on wall properties (like elasticity).

2.2.2 Individual Tube models

The tube model is another important basis for the present research work and describes a pressure transfer function of the brachial artery to aorta for blood pressure, based on distal load and local arterial behaviour. Tube model methodologies, which are based on anatomy and uniform tube models show an interesting results that the transfer function from brachial artery to aorta can be simply based on a lossless uniform tube. This is very useful for developing the present research simulation model in that the outcome indicates that arterial tapering is only a minor factor. The peripheral bed, i.e., the Windkessel parameters, are of limited influence on the pressure transfer: it has been found that changes in peripheral resistance, which can vary over a wide range, had only a small effect on systolic, diastolic, and pulse pressure. In consideration of Westerhof et al. [32], we conclude that there is one shortcoming which is that they did not evaluate the influence of heart rate or other cardiac factors. Also, there are two unanswered questions, firstly, that to conclude whether or not a generalised transfer function can be used for other models. Secondly, is it possible that the individualised transfer function will improve the calculation of central pressure, when the travel time is measured, preferably noninvasively [32]?

To assess pulse transit time and wave reflection alone from the pressure waveform can be done through non-invasive methods. The method of triangulation approximation of flow wave assessment is proposed by Westerhof et al. [34], while Qasem et al. [35] proposed, to verify the assessment from recording through a single pulse for aortic pulse wave velocity and to explore the estimation through pulse wave velocity and the Reflection Method (RM). This is very important for the present research as it does apply non-invasive external forced oscillations on the phantom aorta under study. In considering Kips et al. [36], our conclusion is, the study is entirely based on noninvasively measured data, and the quantification of wave reflection, by using a triangular flow wave approximation, shows limited accuracy when applied to noninvasively measured pressure and flow data [36]. Therefore, an important question remains regarding whether not there was the need of invasive methods to improve the approximation method.

Testing of nonlinear, one-dimensional (1-D) equations of pressure and flow wave propagation in conduit arteries against a well-defined experimental 1:1 replica of the human arterial tree

provides greater accuracy during simulation. The experimental model and numerical model based on 1-D equations reproduce the main features of the pressure and flow wave propagation which builds the confidence in the present research for large artery of human cardiovascular system. The 1-D formulation and numerical model, based on the geometry wall compliance and boundary conditions of the system are used for mathematical simulations. In consideration of Matthys et al. [46] we concluded that the effects of curvature of the vessels can be neglected. However, the significance of the effect of the viscoelasticity of the silicone wall on damping peripheral oscillations is unanswered. The present research uses a silicone wall: Dragon Skin® 10 refer to Appendix D for more detail.

2.2.3 Windkessel models and functional arterial parameters: stiffness and resistance

In cardiovascular events arterial pressure plays an important role. Arterial parameters like stiffness and resistance, and the pressure response are an important part in treatment of hypertension. The variables which are most often related to cardiovascular events are pressure systolic (Ps), pressure diastolic (Pd), and pulse pressure (PP). Also, there are other variables obtained such as pressure augmentation and waveform analysis along with inflection and shoulder points. The variables obtained can be in combination or alone in order to give event prediction [26]. The forward (Pf) and backward (Pb) pressure can be separated by wave separation. Both Pf and Pb, along with the reflection index and magnitude and the return time of the reflected wave can be derived assuming the tube structure of the arterial system. The complete description of the arterial system is given by input impedance. As input impedance is not easily derived, impedance can instead be described by arterial stiffness together with aortic characteristic impedance (Z_c), arterial stiffness (ET), and systemic vascular resistance (SVR). In [26] input impedance was calculated from aortic pressure and flow by using Fourier analysis. The three parameters SVR, ET, and aortic Z_c were derived by fitting the Windkessel impedance to the input impedance data. Using measured flow in patients, the pressure was then calculated from flow and the three arterial parameters to obtain predicted pressure. Predicted pressures were compared with measured pressure. The results were all pressure-derived variables and gave limited information on arterial function in terms of stiffness and resistance. Input impedance is accurately described by three parameters: systemic vascular resistance, total arterial stiffness, and aortic characteristic impedance [26]. The investigation shows relations between pressure-derived variables and arterial stiffness in aging, and focus on how aortic pulse wave inflection point, augmentation index, and reflection magnitude do not allow the estimation of functional

arterial parameters like stiffness and resistance. This is a significant point for the present research [26] as the applied forced oscillations at inflection point impact on the descending aorta. As the descending aorta will be our point of inflection to see the impact response at ascending aorta. Brachial arteries in healthy and diseased cases have been simulated experimentally and pressure and pressure gradient waves have been studied by considering an open loop hydraulic system comprising of some of the major components:

- (1) An elastic element (the Windkessel element) placed before and coupled to the elastic tube,
- (2) The elastic tube.

The results show that for a healthy heart, the pressure rise was more noticeable at higher viscosities. However, the amplitude of the pressure wave decreased with increase in viscosity. The pressure drop increased with increase in the viscosity, as the pressure gradient wave possessed higher values. With the use of rigid segments, stiffening of this element dramatically reduced the amplitude of the pressure wave compared to the elastic state (refer figure 2).

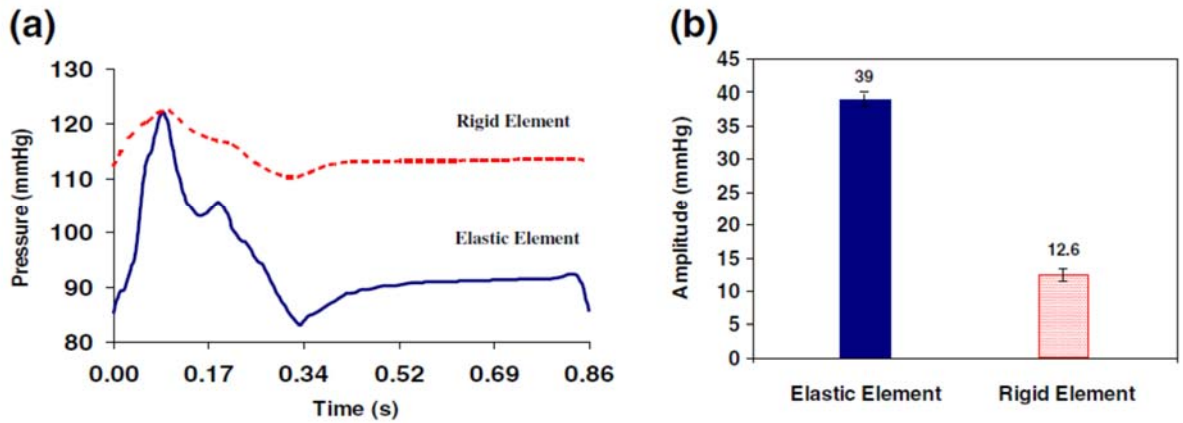


Figure 2: Windkessel effect of elastic and rigid element: (a) Pressure (b) Amplitude [29]

Nichols et al. [43] considered the interaction between the heart as a pump and the arterial system as its load, and pulsatile arterial wall stress along with the elasticity of the aortic tissue. We conclude from this paper that the Windkessel effects on central arterial waves can occur with or without a reduction in mean arterial pressure, peripheral vascular resistance and stiffness of arterial wall [43]. To give better results, the elasticity of the phantom aorta material has been taken into account for the present research.

The haemodynamic parameters for healthy humans, such as Windkessel element stiffness, wall stiffness and viscosity, have significant effects on the waves, propagation of waves and the

patterns of the waves, as demonstrated by experiment. In future this model can be used to simulate blood flow in different conditions, in conjunction with a numerical model.

In considering the findings of the Anssari-Benam et al. [29] we conclude that there are few interesting shortcomings:

- (a) The results were obtained using a Newtonian fluid; whereas, the blood is a non-Newtonian fluid. The blood has higher viscosity in smaller vessels which have lower flow rates, i.e., capillaries and arterioles. Studies have been conducted which suggest to assume the blood as a Newtonian fluid, which gives the results within the acceptable range of accuracy for larger arteries [30]. Such assumptions have been considerably used both in computational simulations and experimental analysis.
- (b) There is a limitation in sampling time resolution (0.01 s) due to this the precise value of the time shifts were not observed between the waves in rigid and elastic conditions.
- (c) There was a difficulty in direct use of the Moens-Korteweg equation [31] for calculating theoretically wave propagation times in this study. It is due to the fact that the tube wall in study was 0.9 mm, which is not theoretically a thin-wall tube. Also, silicone rubber is theoretically a compressible material with a Poisson ratio of $\nu = 0.4$. So, these two characteristics violate the assumptions used in deriving the Moens-Korteweg equation.

$$c = \sqrt{\frac{Eh}{2\rho a_i}} \quad \text{where } c \text{ is the wave speed, } E \text{ is modulus of elasticity, } a_i \text{ is inner radius}$$

and ρ is the density of fluid.

2.3 Cardiovascular System Biomechanics

The important question investigated in this literature survey is about how to address and validate new algorithms to efficiently predict the hemodynamic in large arteries. All methodologies used include Fluid Structure Interface (FSI) between the blood flow and the arterial wall. The blood is modelled as a Newtonian fluid whereas the aortic wall is considered a linear elastic structure. In consideration of Crossetto et al. [39], we conclude that there are issues with simulation that does not take fluid–structure interaction into account [39]. In the present research fluid structure interaction is modelled with Mathematica code for a simulated cardiovascular system with the phantom aorta.

The geometry and material properties of the aorta are used to formulate Boundary Value Problems (BVPs). The physiological implications of the biomechanical analysis is important in the cardiovascular system. The homeostasis of the vessel wall has implications on growth,

remodelling and postnatal development. The methodology used is Fung's (1993) [44], biomechanics approach on the aorta. The methodology serves as the foundation for choosing the material properties and geometry of the major artery aorta. In consideration of Kassab [45], we conclude that the constitutive equation for the vascular smooth muscle is critical. However, a simplified mathematical simulation model has been made and tested as phantom aorta in this research based on geometry and linear elastic material properties somewhat similar to that of human aorta [45].

The effects on wave propagation, due to nonlinearity and viscosity in an elastic axisymmetric vessel impacts on the fluid flow in the system. It is assumed that the fluid is flowing in a laminar flow with further assumption as an incompressible and Newtonian fluid by use of power series and Fourier series to solve the mathematical equation. Three types of models such as;

(a) Linear model (b) Nonlinear model and (c) Lighthill comparison have been used to develop an algorithm in 2D. In consideration of Park et al. [40], our conclusion is the viscosity is more significant than wave propagation due to nonlinear and viscous effects. The present research utilizes coloured water fluid [40] which has low viscosity.

2.4 Recent Work on Active Forces at AUT

The application of the vibrations affects the whole aorta. In [44] rat aortic muscles were used to observe the application of sinusoidal or smooth vibrations along with the use of KCl-Potassium Chloride chemical stimulus. The research output was that there is a continuous reduction of active forces which leads to relaxation of aortic tissue [44].

The above study gives a good idea about application of vibrations. This provides more impetus for the present research work, to study the effects of forced oscillation on the simulated human aorta with validation through phantom aorta. The present research work is based on the forced oscillation being applied at the descending point in the phantom aorta of human being and observing the output effects both at descending and ascending aorta.

The core concept for the development of a model based on fluid flow in pipe with constant diameter. However, very few arterial models incorporate external forces. In consideration of Chaudhry (1987), [49], Elansary et al. [50] and Reddy et al. [51], we conclude that our present mathematical equation has been derived with an applied force component which is vital for the present research.

2.5 Objectives

The main objectives of this work is to study the effect of induced/forced oscillations on a simulated normal human aorta that is a phantom aorta. A forced oscillation will be applied at the descending phantom aorta, the response of the pressure and flow due to the pulsating nature of the blood at both descending and ascending aorta will be studied.

2.5 Thesis Structure

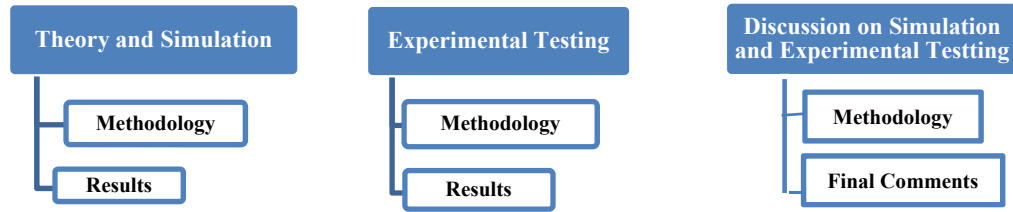


Figure 2.1: *Thesis structure*

The thesis structure shown above covers the research activities. It starts with a brief introduction, literature review and then it follows the flow as shown in figure 2.1. The first part of the thesis is the theory and simulation, the second part is experimental testing. The theory and simulation will give the foundation of the research. The methodology starts with the derivation of the mathematical equations considering pipe flow and subsequently develops the simulation models using the Wolfram Mathematica®10 (Wolfram Research of Champaign, Illinois, USA) [57]. In experimental testing, the methodology starts with the experimental testing done on the cardiovascular simulation set up with phantom aorta. The results obtained from both theory and simulation and the experimental testing will be discussed in the discussion chapter in detail and last chapter presents conclusion with future scope from this research.

Chapter 3: Theory and Simulation

3.1 Introduction

This chapter describes the formulation of a theoretical model that describes the system of phantom aorta in which is induced forced oscillations. The mathematical model will be used as the foundation of a simulation for this research. The results obtained by simulation will be compared with results from an experimental set up with varying diameters, areas, lengths and also different amplitudes and frequencies of the forced periodic oscillation.

The model is based on fluid flowing in a pipe, analogous to the human aorta, which has blood as fluid flowing through it. Flow is assumed to be periodic.

3.2 Mathematical Model

The partial differential equations describing the conservation of mass and momentum for one-dimensional, transient flow through a pipe with slightly deformable walls as shown in figure 3.1 are given below (Chaudhry 1987):

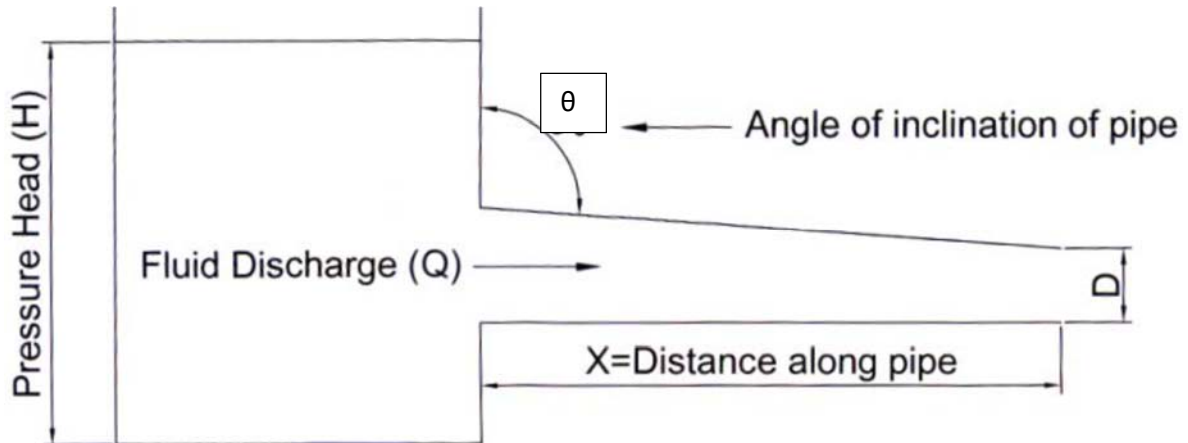


Figure 3.1: Transient flow through a pipe

H is the pressure head, Q is the discharge, g the acceleration due to gravity, θ is the angle of inclination of pipe, f is the friction coefficient, D is the internal pipe diameter, A is the cross-sectional pipe area, c is the pressure wave velocity, x is the distance along pipeline, and t is the time.

$$\frac{\partial H}{\partial t} + \frac{c^2}{g A} \frac{\partial Q}{\partial x} = 0 \text{-----} (1)$$

$$\frac{\partial Q}{\partial t} + gA \frac{\partial H}{\partial x} + Ag \sin \theta + f \frac{Q|Q|}{2DA} = 0 \text{-----} (2)$$

The above equations have been modified further to get the requisite equations.

From Conservation of mass:

We get the following equations (Reddy et al, 2010);

$$-\frac{\partial A(t)}{\partial t} = A(t) \frac{\partial v[x,t]}{\partial x} \text{-----} (3)$$

Using (3) we get,

$$-k \frac{\partial p}{\partial t}(x, t) = A(t) \frac{\partial v[x,t]}{\partial x} \text{-----} (4)$$

From Conservation of Momentum, we get the following equation (Reddy et al, 2010);

$$\frac{f_{external}}{A(t)} - \frac{\partial p}{\partial t}(x, t) = \rho \frac{\partial v[x,t]}{\partial x} \text{-----} (5)$$

The final equations relate external force application to pressure and flow with diameter and area.

Equations (2) and (5) will give the following equation.

$$\frac{f_{external}}{A(t)} - Ag \sin \theta - D \frac{\partial p}{\partial t}(x, t) = \rho D \frac{\partial v[x,t]}{\partial x} \text{-----} (6)$$

Where

$$A(t) = A, k = \frac{A}{\rho c^2};$$

$$c = \sqrt{\frac{hE}{\rho D}} \text{ [31]}, h = \text{height of Aorta}, E = \text{Young's Modulus}, \rho = \text{Density of blood},$$

D = diameter

The set of equations consisting of (5) and (6) needs to be numerically solved by a mathematical tool or software like Mathematica [57]. This is presented in the simulation section 3.3 in the present chapter

Inference

Equations 5 and 6 can be used to describe the travelling pressure and flow waves from descending aorta to ascending aorta in response to applied forced oscillations $f_{external}$ at the descending aorta point and this is the core area of this research. The mathematical equation simulation model will give the output response to the different forced oscillations applied with variable frequencies

and magnitude which will be compared with phantom aorta in the experimental set up in chapter 4.

3.3 Methodology - Simulation Model

This section will discuss in detail the methodology used to simulate the mathematical model developed above. The simulation was performed using Mathematica[®]10 [57]. Simulations of various models under different scenarios were performed.

Equations 5 and 6 given in section 3.2 describe the output response of the pressure and flow to the applied forced oscillations. For this reason, the simulation will be carried out using a lengthwise segmentation of the aorta. The descending aorta is assumed to be the point of application of the forced oscillations in order to see the effect at the ascending aorta. Also, segmentation describes the diameter changes, which increase towards the ascending aortic arch. Each segment is simulated separately and the output of the first segment becomes the input of the next segment, which allows simulation of waves from the external and cardiac oscillations travelling throughout the descending and ascending aorta. The response at ascending aorta is a reflection of the summative effects of each segment. Geometric parameters like diameter and the length of the aorta were taken from the medical literature and experimental setup geometry from other research groups [28].

Simulations were performed using different conditions of pressure and/or velocity boundary conditions at the descending aorta, and external forced oscillation with different frequencies, and amplitude. For each case the output was observed. Mathematica code for the simulations are given in Appendix A.

3.3.1 Model Geometry

The geometry adopted for the model is given in the table 3.1 and below.

Table 3.1: Initial test simulation model geometry of phantom aorta [56]

Aorta Geometry	Size (mm)
Wall thickness (H)	1
Diameter (D1)	25
Diameter (D2)	20
Length (L)	750

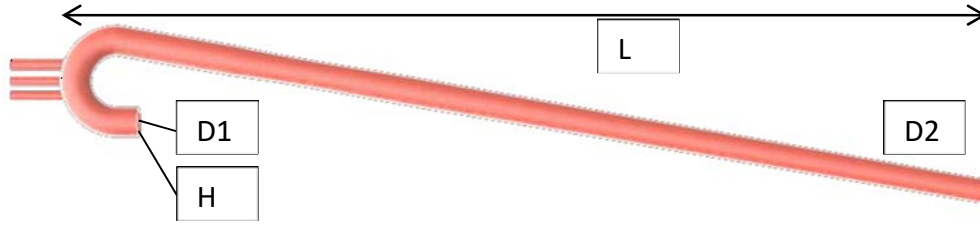


Fig 3.2: Phantom Aorta [56]

For simulation purposes, tapering between D1 and D2 was considered to be variable diameter and 10 divided segments were used to describe the full length of the aorta. Segment diameters were interpolated, but each segment itself was considered to be a ring.

3.3.2 Different Simulation Scenarios

Table 3.2 below, shows a comparisons of all the simulated scenarios and their applied signals.

Table 3.2: Comparisons of all the scenarios with their applied signals.

Model -Scenarios	Boundary Conditions		Applied Oscillations
	Pressure	Velocity	
Initial Test Model	Yes	Yes	No external applied oscillations
Scenario 1	Yes	Yes	Sine wave
Scenario 2	Yes	Yes	Impulse
Scenario 3	Yes	Yes	Forced oscillations with different frequencies and amplitude
Interpolation	Yes	Yes	Curve fit of pressure waveform
Beat signal	Yes	Yes	Another pressure waveform

Scenario 1

The first scenario was used to check the effect of forced oscillation of sine wave input at the descending aorta with variable frequencies and amplitudes.

Scenario 2

In scenario 2, the impulse signal was applied to test and to check the output response of both descending and aorta pressure and flow.

Scenario 3

The scenario 3 is the final refined model using a physiologically realistic pressure with interpolation and beat. The details of the Beat code are given in the appendix A. The signal was constructed from a sampled signal recorded from the signal shown in figure 3.9. This made the research output more meaningful. In order to be used in the simulation, an interpolation function

was constructed (refer figure 3.8), the detailed Mathematica code of the interpolation used in this research is provided in the Appendix A.

3.4 Results

For Model 1 refer figure 3.3 below.

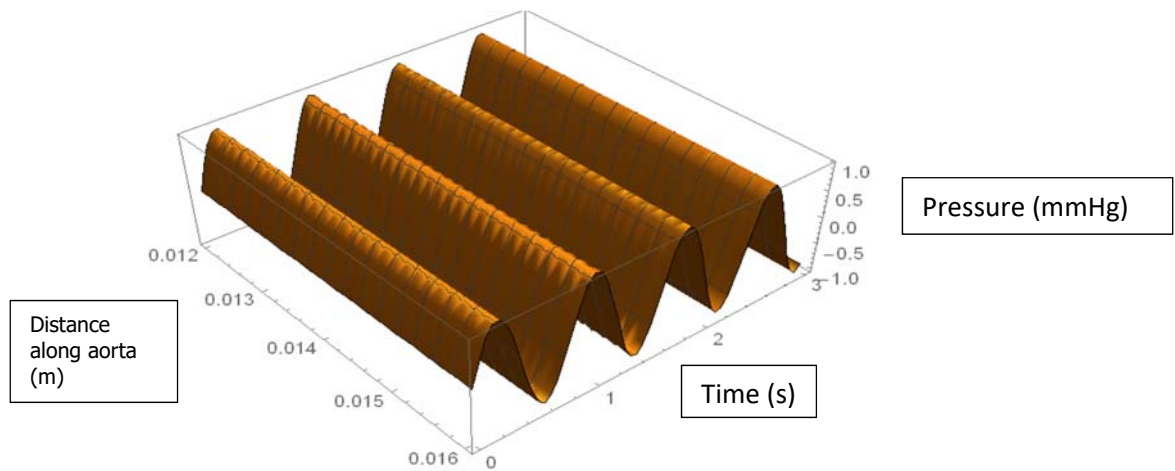


Figure 3.3: Model 1 Sinewave - Pressure

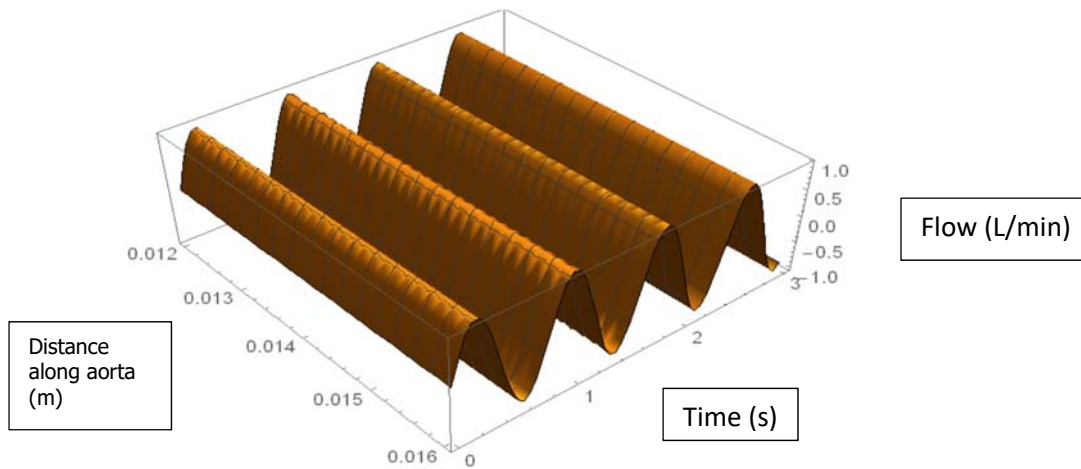


Figure 3.4: Model 1 Sinewave - Flow

The figures 3.3 and 3.4 are the result of the first simulation which shows the wave shape which is a travelling wave similar to sinusoidal wave. The tapered segments have been considered for the simulation. The results show in the simulation when sine is applied to the model it gives out sine wave of both pressure and flow.

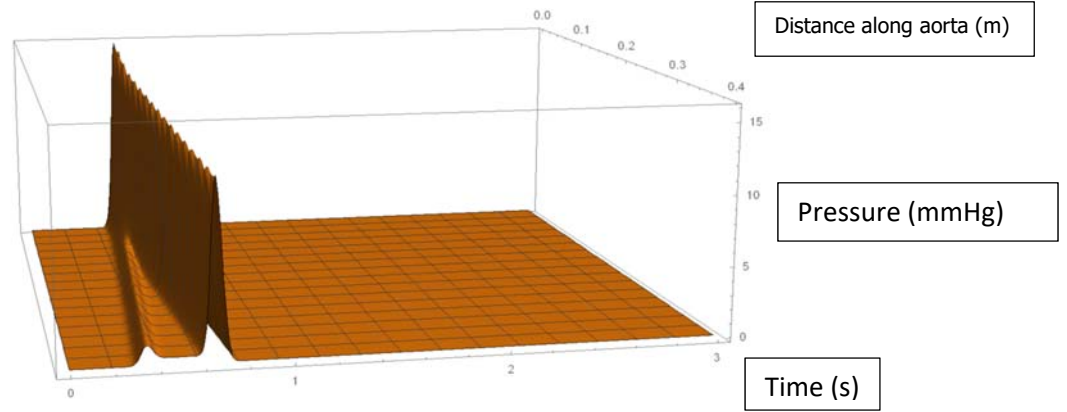


Figure 3.5: Impulse signal

The figure 3.5 shows an impulse signal response. The impulse output response gives the expected result with the application of the impulse signal. This result gives the confidence in the simulation model responding well to the applied signal, the change in applied input signal in the simulation was responded well by showing changes in the response of the output signal, hence verifying the mathematical model is working in the different simulated scenarios.

In scenario 3 the final model has two output signals (figure 3.6 and 3.7) along with interpolation and beat signal in figure 3.8 and 3.9. The interpolation is used to fit the signal whereas the beat represents one heart cycle which has all the information and can be repetitive.

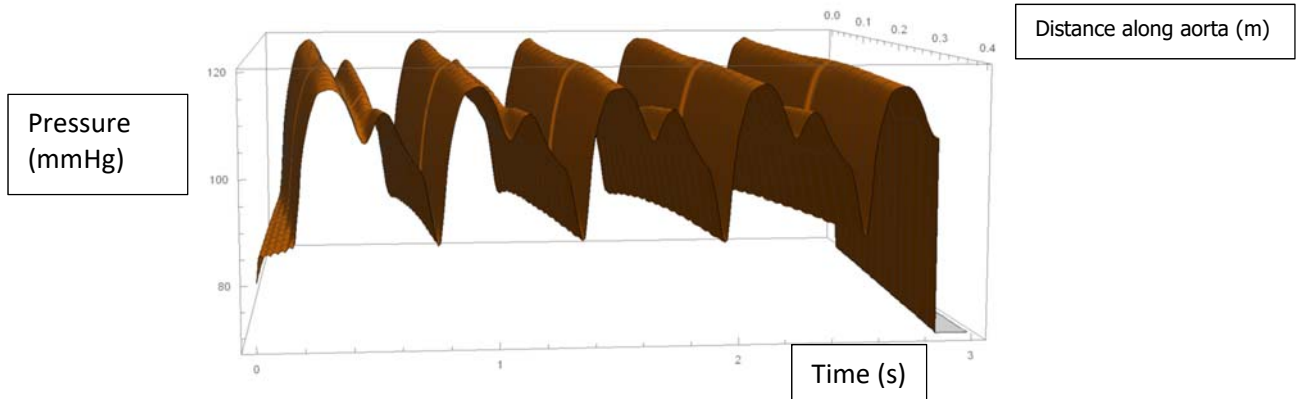


Figure 3.6: Model without beat

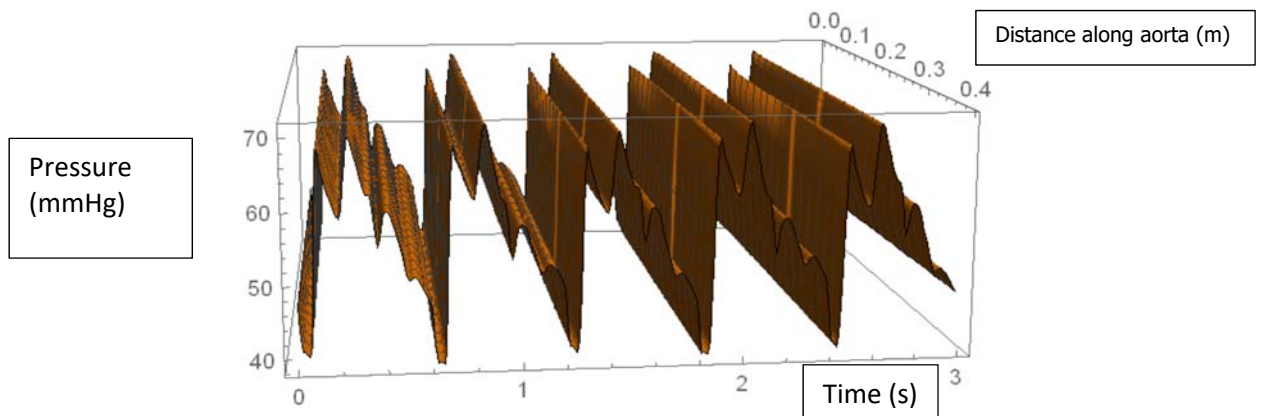


Figure 3.7: Final Model with beat and interpolation

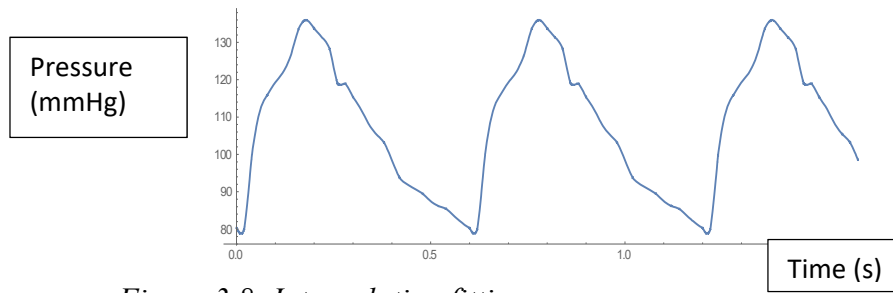


Figure 3.8: Interpolation fitting

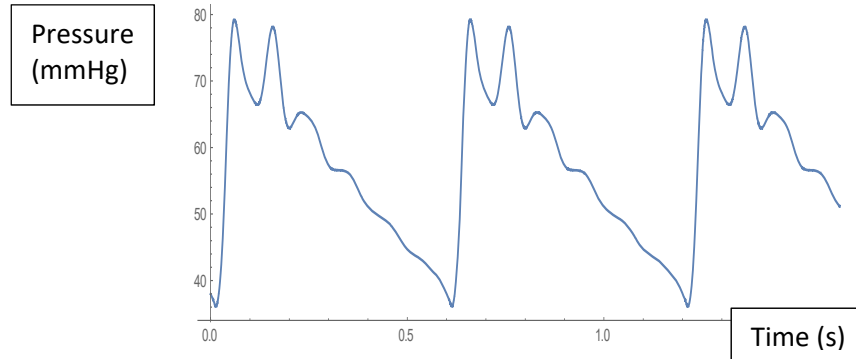


Figure 3.9: Beat signal

The results obtained from the simulation are firstly, to check whether the mathematical equations mentioned in the section 3.2 is responding to the simulated applied forced oscillation signal. It showed significantly the effects of the applied forced oscillations with different frequencies and magnitude; this gave confidence in moving further to the experimental stage. The simulation results for each applied input signal showed the mathematical model gave the expected results. The next stage is the experimentation stage to validate the simulation results.

Chapter 4: Experimental Analysis

4.1 Introduction

An experimental analysis was performed to compare with the simulated mathematical model for the effect of forced oscillation on the cardiovascular simulated system with phantom aorta for validation. The experimental set up for this research was based on an arterial phantom test rig developed for other research experiments. The details are given in the 4.3.5 section for the initial experimental set up and then a subsequent modified set up that has been used for the remaining experimental set up for this research.

4.2 Aim

The main aim of the experimental analysis is to observe the effects of different frequencies and the amplitude of the applied forced oscillation on phantom aorta. This allows comparison of the experimental results of pressure and flow in the phantom aorta with the simulated model developed in the previous chapter.

4.3 Methodology

An experimental phantom model has been used as the basis of the experimental analysis.

4.3.1 The Phantom Aorta

The importance of the phantom model is to simulate the experimental related studies of medical treatment under well-defined parameters [53]. Phantom aortas are developed in order to simulate both biophysical properties and blood vessel structures, which are similar to the real human heart aorta or structures or organs. Silicone blood vessel phantoms are widely used in research studies. An example of rapid prototyping of aorta models based on silicones for validating simulation is [53], according to Savrasov's et al, to improve the pressure and flow waveform at the point giving waveforms which better represent physiological characteristics. There was a suggestion of tapering the aortic diameter. This was the variance of pressure and flow waves along the aorta which were observed when the operation of the cardiovascular simulation was carried out [54]. The phantom aorta used in this research was based on Johnson's work [55]. It was constructed using Dragon Skin[®] 10 in Appendix D.

4.3.2 Aortic Geometries

From Johnson's work the aortic geometries for the ascending aorta is to be approximately, Ø25 mm and the descending aorta is about Ø20 mm [55]. The length is around 700 mm and thickness is 1 mm. The simple geometry (see Figure 4.1 and Table 4.1) is similar to the present research and Savrasov et al [54].

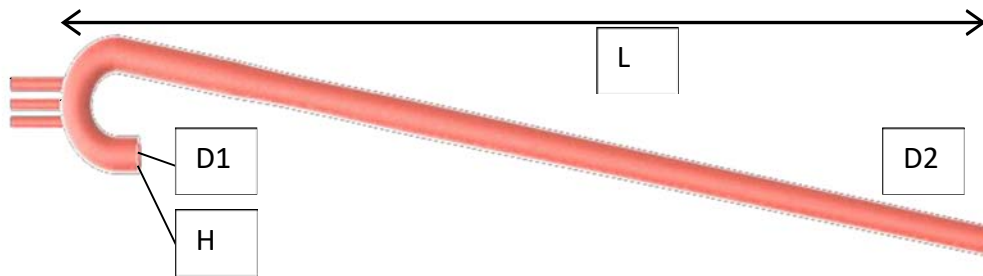


Figure 4.1: Johnson's phantom aorta shape [56-58]

Table 4.1: Dimensions of the aorta shown in Figure 4.1 [56-58]

Aorta Geometry	Size (mm)
Wall thickness (H)	1
Diameter (D1)	25
Diameter (D2)	20
Length (L)	750

In this research, the length of the aorta has been modified to 500 mm as this more closely matches physiological dimensions, as mentioned in the simulation section.

4.3.3 Materials

The phantom aorta has been made from the material called Dragon Skin[®] 10 [58]. It is a platinum cured silicone rubber. It is used for the aorta with 1:1 ratio of Platinum curing agent and Dragon Skin[®] 10. This is the material used in the research.

4.3.4 Aorta Phantom Experimental Simulation Setup

Testing and validating the effects of forced oscillation on the normal human aorta, the application of induced oscillations at the descending aorta, and to see the effects at both descending and ascending portion of the aorta, was achieved by measuring the aortic pressure and flow. The initial set up was prepared by another research group at IBTec by Jones [56] was used as a starting point for this experimental set up and subsequently it was modified to get the

required output for the discussion of this research. The modifications are shown in figure 4.13. The initial set up is shown in the figure 4.2 for the initial Cardiovascular Experimental Simulation setup hardware that integrated the phantom aorta to complete the setup.

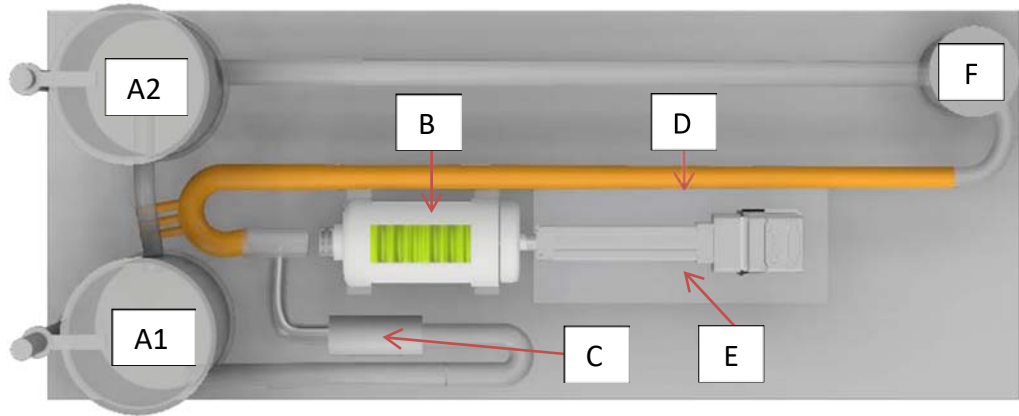


Figure 4.2: (A1): Reservoir 1. (A2) Reservoir 2. (B): Bellow system. (C): Valves. (D): Phantom aorta 2. (E): Linear actuator. (F): Capillaries [56].

4.3.5 Design and Operation

The figure 4.2 shows the hardware part of the initial set up of cardiovascular system. The setup was easy for mounting of hardware components. The SmartMotor™ (MOOG Animatics, United States) linear actuator uses the programme code in Appendix B. Care has been taken to reduce the force required to actuate the linear drive motion of the experimental set up by using bellows. Bellows have negligible frictional force when in operation. The type of bellows selected is a suction cup which has six-folded bellows by piGrip® [56].

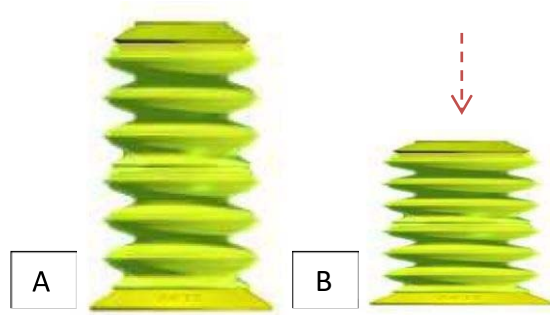


Figure 4.3: (A): piGrip® bellows uncompressed. (B): piGrip® bellows compressed [56]

The piGrip® bellows is fitted inside a 3D printed frame along with bush and coupling shown in the figures 4.4 and 4.5.

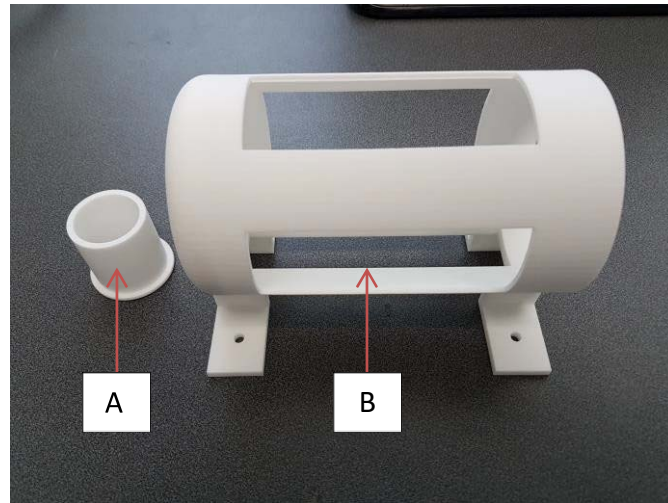


Figure 4.4: (A): 3D printed bush. (B): 3D printed frame for the piGrip® bellows [56].

The piGrip® bellows was connected to the mainframe by a bush. The main function of the mainframe is to hold piGrip® bellows components to the main base of the experimental setup refer figure 4.5 below



Figure 4.5: The piGrip® bellows along with coupling and bush [56]

Two 1.5 L liquid containers served as reservoirs. The reservoirs provide the liquid flow through the cardiovascular simulation setup and phantom aorta. The reservoirs are flexible, providing both up and down movement to change the calibration pressures of the liquid (refer figure 4.6). All the hose connections to and from the reservoirs were 12 mm in diameter.



Figure 4.6: The reservoirs of 12 mm diameter hose connections.

The figure 4.7 shows two one-way brass check valves (A) attached to the entry and exit of the bellows system to maintain the flow of liquid. The other components were, prosthetic aortic valve (D), shown in Figure 4.7, to control the liquid flow in the aorta from the heart connected into PVC pipe connections shown Figure 4.6.

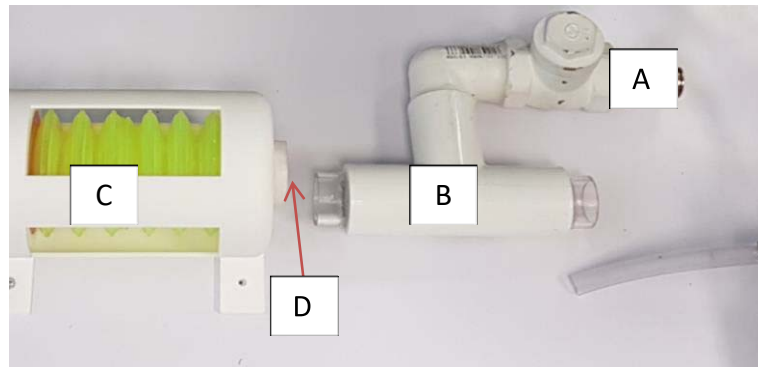


Figure 4.7: (A): Brass check valve. (B): PVC piping. (C): Bellows system. (D): Aortic valve [56].

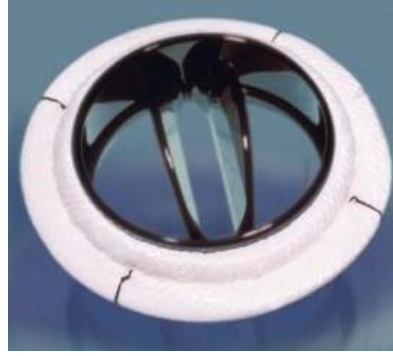


Figure 4.8: Prosthetic aortic valve (CardiaMed Rotating Heart Valve) supplied by OBEX®

The simulation of the capillaries were made by the artificial capillary bed. The main objectives of the artificial capillary was to increase the pressure inside the phantom aorta and to restrict the flow of water. This was done by inserting a cylindrical shaped sponge at the end of the phantom aorta, with diameters of Ø30 mm x 20 mm with 12 mm push fittings through PVC pipe (figure 4.9).

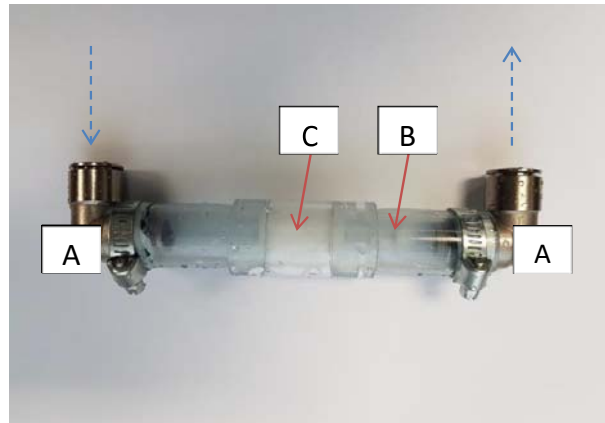


Figure 4.9: Artificial capillary system. (A): 12 mm push fitting. (B): PVC pipe. (C): Cylindrical sponge [56]

The pump mechanism was controlled using a camming profile that was loaded on the SmartMotor™. The main function of linear actuation is to make the SmartMotor run smoothly for pumping the fluid into the cardiovascular simulation setup.

As shown in figure 4.10. The profile was designed to mimic the output flow of the left ventricle at a cycle rate of 60 bpm that compresses the piGrip® bellows by 34 mm.

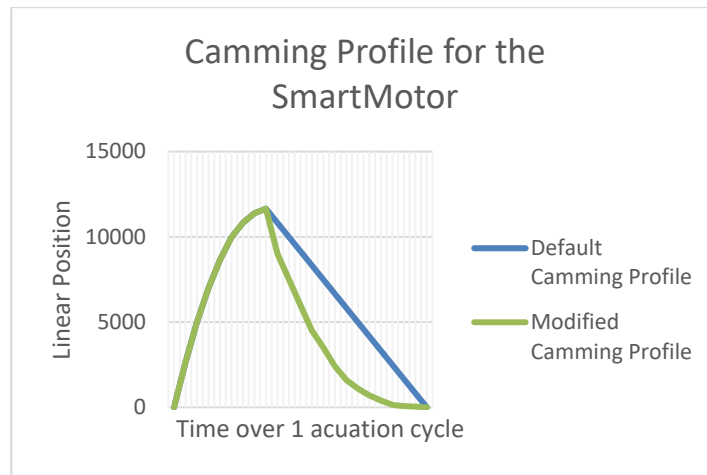


Figure 4.10: Camming profile was uploaded to the SmartMotor™ (MOOG Animatics, United States).

The camming profile's linear position set up is done through the SmartMotor™ program code given in the appendix B

When the setup of all hardware components was established, along with the software instructions loaded properly, testing began to check the reliability and proper functioning of the Initial Cardiovascular Experimental Simulation Setup. The testing included the measurement of pressure and flow at different points in the phantom aorta.

4.4 Modifications to introduce mechanical displacements

The cardiovascular experimental simulation setup was modified in order to introduce mechanical displacements at the descending aorta.

The following changes in the setup were made. The modified equipment is shown in figures 4.11a and b. From figure 4.11a, the phantom aorta was used for this research. The Transonic Flow meter is to measure the blood flow. An Amplifier is used to amplify the signal generated from the output response in both descending and aorta. The SmartMotor™ is used to pump the blood into the system. The figure 4.11b is the modified diagram, it includes an LDS® V406 shaker (figure 4.12 below) which is very dependable and versatile. The LDS® V406 shaker features a usable frequency range from 5 to 9000 Hz. This was used along with an LDS® PA 100E power amplifier to induce the oscillation through vibration from the shaker. The modified schematic diagram of cardiovascular simulation system along with the phantom aorta is shown in figure 4.11b. The detailed technical specifications of the LDS® V406 shaker is given in appendix C.

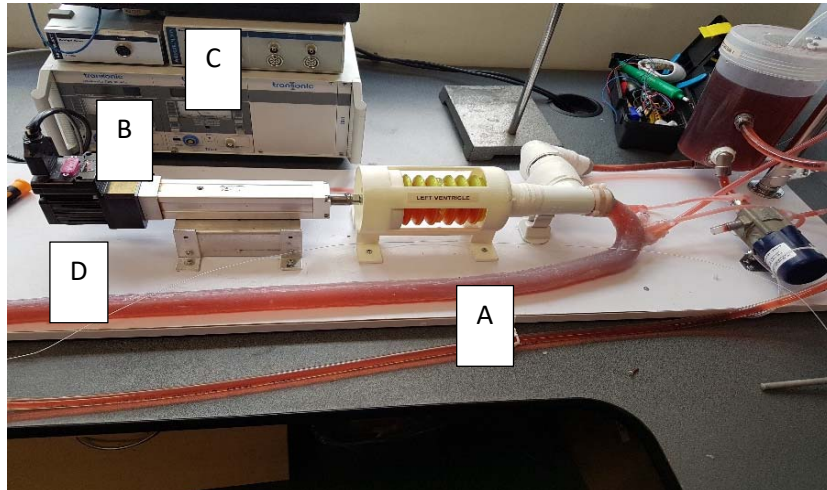


Figure 4.11(a): Initial Modified experimental setup: (A) Phantom Aorta. (B) Transonic Flow meter. (C) Amplifier. (D) SmartMotor™



Figure 4.11(b): Initial Modified experimental setup: (E) LDS® V406 shakers



Figure 4.12: LDS® V406 shakers

Figure 4.13 below shows the detailed schematic modified diagram for the present research for the forced oscillations needed for the measurement of pressure and flow of blood in the phantom aorta

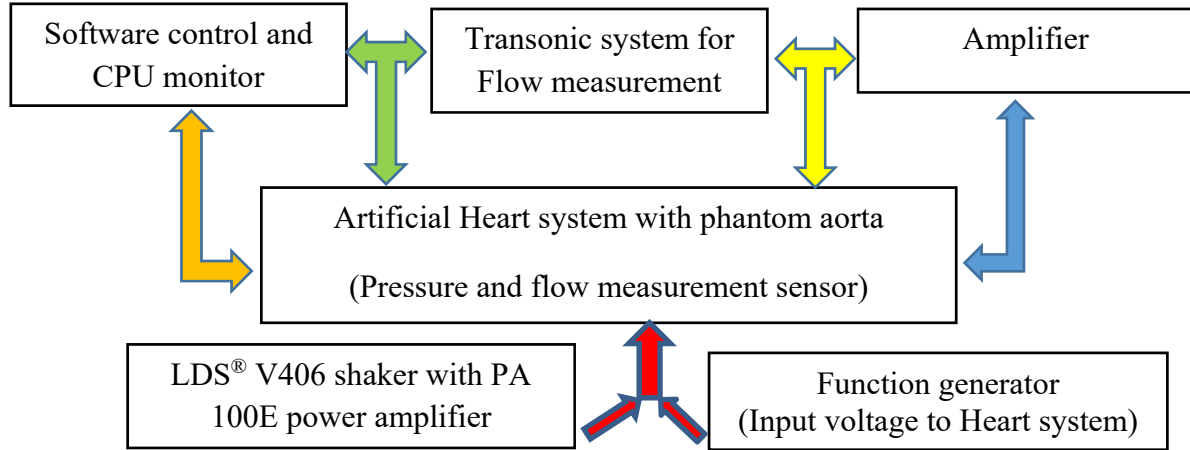


Figure 4.13: Initial modified schematic block diagram of cardiovascular simulation setup

Legend

Orange Interactions of Software controlled and CPU monitor

Green Interaction transonic system with Artificial Heart system and Software controlled and CPU monitor

Yellow Amplifier together with transonic system and Artificial Heart system

Blue Amplifier with Heart system and then with transonic system

Red Function generator (Input voltage to Heart system) along with LDS® V406 shaker and 100E Power amplifier

The modified set up used for measuring the pressure and flow with forced oscillations is a key area of this research. The operation of the above system is described below:

Referring to figures 4.11a & b, 4.12 and 4.13, the Artificial Heart System with phantom aorta is operated by SmartMotor™-which is programmed controlled. The motor operates in a way to simulate the heart pulse rate. The interaction between the Artificial Heart System, which is software controlled, and CPU monitor is shown in orange colour. The cardiovascular simulation platform gives pressure and flow waveform by using Transonic flow and PowerLab (ADInstruments, USA) measurement devices which uses a Millar MicroTip catheter for pressure measurement. The signal interaction is shown with green, yellow and blue colours to indicate interaction with the Artificial Heart system and PC. The waveform is collected in

LabChart (this will be discussed in results in detail). The entire system input is operated through external forced oscillation (LDS[®] V406 shakers, LDS[®] PA 100E power amplifier and function generator) and shown in red colour. The measurement was subject to a low pass filter up to 50 Hz.

Table 4.2: Measurement equipment used for cardiovascular simulation set up

Parameters	Measurement Equipment	Company
Forced Oscillations	LDS [®] V406 shakers, LDS [®] PA100E, Function Generator AFG3102C	Bruel and Kjaer and Tektronix
Pressure	MikroTip [®] cathether, SmartMotor [™]	Millar and MOOG Animatics
Flow	Perivascular Flow Module	Transonic
Force Displacement	Force Displacement Transducer	

The table 4.2 gives the information about the equipment used for the measurement of the pressure, flow and induced forced oscillations in the cardiovascular simulation set up. The detailed technical specifications of each piece of equipment is attached in appendix C

The first measurements were taken with no forced oscillations and secondly, with forced oscillations. Both with no forced and with forced oscillations have been noted and then analysed with the simulated mathematical model. However, there were two setups used: firstly, without submerging the aorta and secondly with submerged aorta. The results of non-submerged aorta exhibited issues due to the experimental setup. The incorrect transmission of the forced oscillation signal into the phantom aorta from the descending part of the aorta, resulted in loss of transmission of the forced oscillations to the ascending aorta. Therefore, the aorta submerged into fluid will give a condition more like in the human body and give a more accurate measurement of pressure and flow as the flow sensors respond well when the aorta is submerged carrying the fluid.

The second set up of the experiment was carried out with the aorta submerged similar to the human body fluid as per the original conditions of the human system therefore, a further modification has been introduced. A further modification was done by introducing a force displacement transducer between the LDS[®] V406 shaker and the artificial capillary with the phantom aorta submerged in the fluid (refer figure 4.14 below).

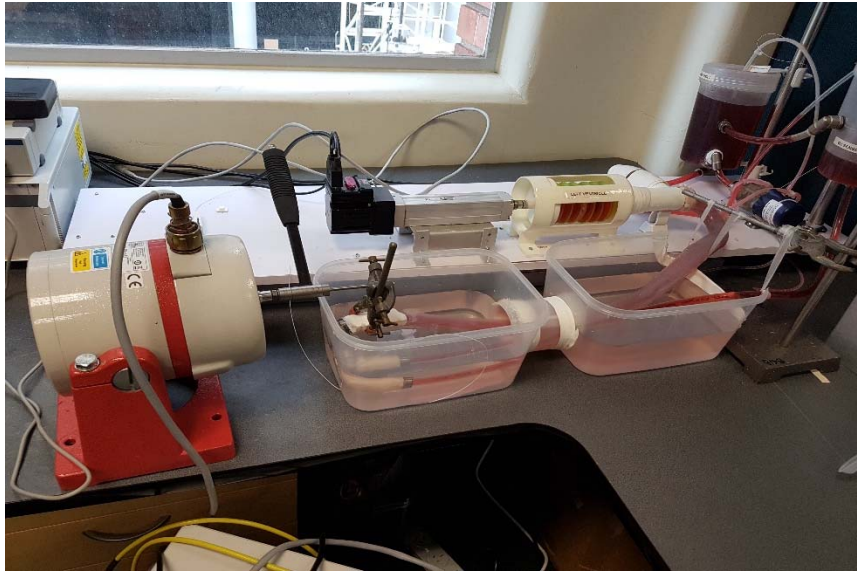


Figure 4.14: Aorta submerged in the fluid

This was needed in order to align the research activities along with the simulated mathematical model. The main function of the force displacement transducer is to transmit the requisite forced oscillations into the phantom aorta from the descending aorta. The observation of the response at the ascending aorta, with the help of the software was used to analyse the output response of the system. It has also been observed that the initial length of the phantom aorta of 750 mm was too long and hence there was another reason for inadequacy in the correct measurement of the pressure and flow at both descending and ascending aorta points in the experimental setup (refer to figure 4.16). At a length of 750 mm, the transmission of the forced oscillation from descending aorta to ascending aorta is not effective. Due to this, the length of the aorta has been reduced to 500 mm.

The reduction in the length of the aorta had a significant impact on the experimental output response which is discussed in the results section (refer to figure 4.16 and 3.25). Please refer figure 4.15 below to see a force displacement transducer in between the phantom aorta and LDS® V406 shaker.

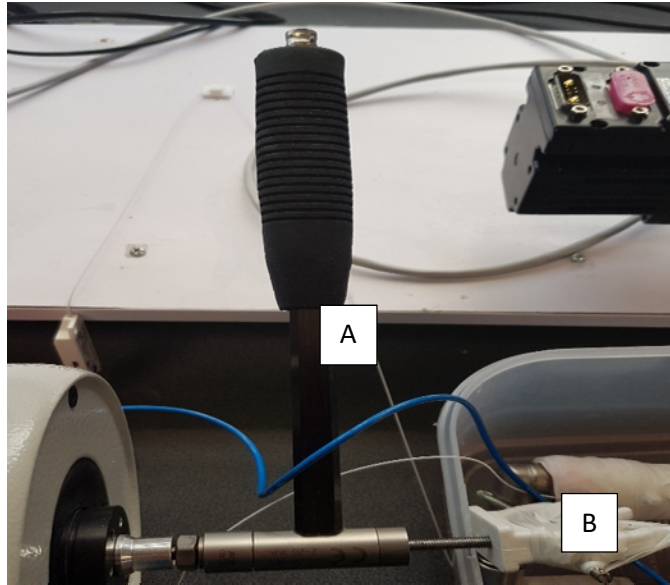


Figure 4.15: (A) Force displacement Transducer. (B) Clamp holding

The introduction of force displacement transducer makes the transmission of the forced oscillations at the descending aorta to ascending aorta effectively close to the simulated mathematical model. All the relevant information is discussed in the results section.

4.4 Results

The results obtained from first the experiment is very significant to this research as it gives very valuable information needed to complete the present research. The first setup results obtained are given in the following figures (figures 4.16 to 4.28).

The results, due to the effect of forced oscillations, are the main basis to get the entire research into the main stream of the title. Figure 3.16 shows LabChart for normal output without any input forced oscillation at the descending aorta and hence no effect on the ascending aorta output. The Blue colour represents descending aorta whereas Red colour represents the ascending aorta.

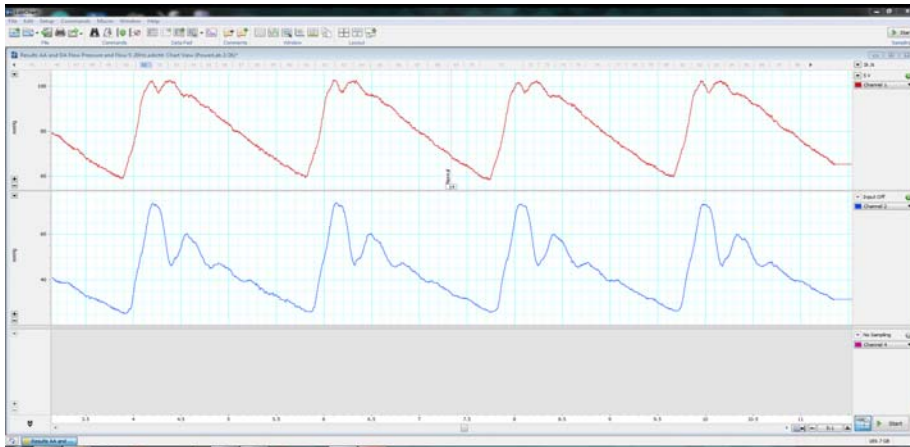


Figure 4.16: LabChart Normal (without any forced oscillations)

The result shown in figure 4.17 LabChart is from the forced oscillation input directly from the function generator.

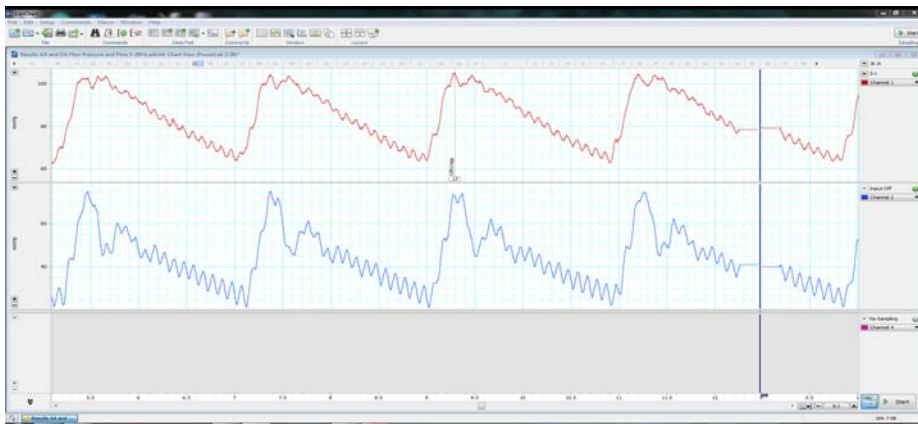


Figure 4.17: LabChart for Sinewave of 10Hz and 1Vpp amplitude forced oscillation direct from function generator

It can be seen that there is a significant change in output response due to the application of the Sinewave of 10 Hz and 1Vpp amplitude forced oscillation direct from function generator, but the measurement was not correct. The forced oscillations were ineffective to transfer the input from descending aorta to the ascending aorta. The output at ascending aorta was very weak.

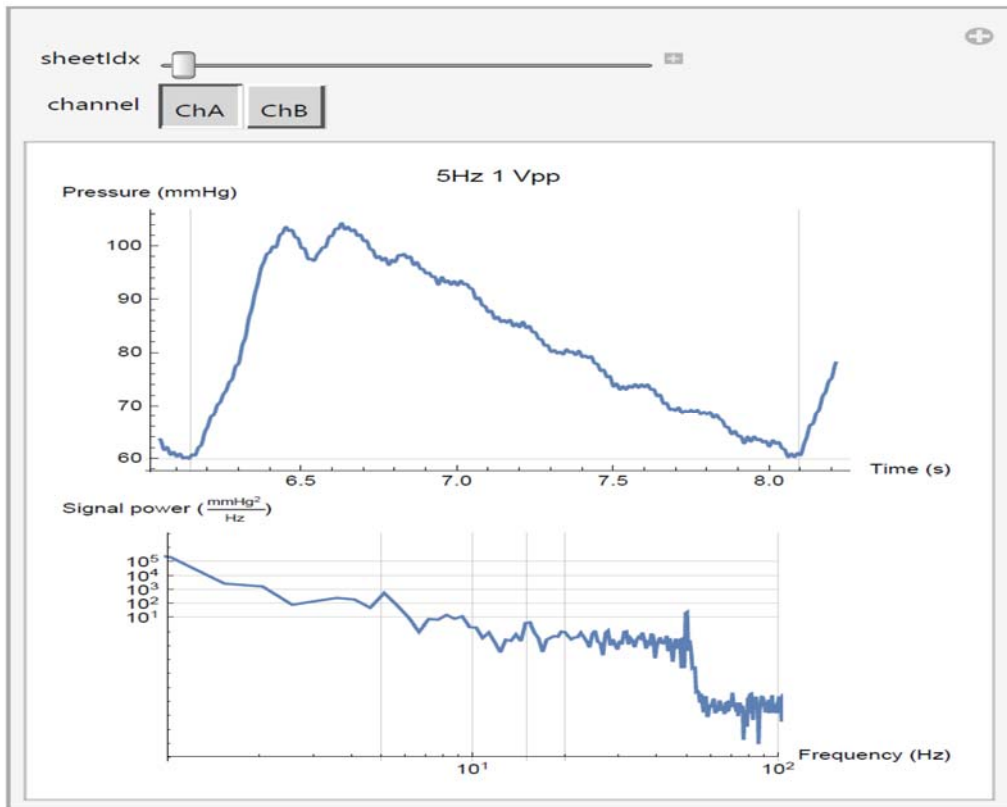


Figure 4.18: Channel A, measurement Spectrum of Ascending Aorta (AO) at 5Hz and 1Vpp.

The first measurement of data gives the response to the force applied at 5Hz frequency 1Vpp amplitude which was measured as signal power in $\frac{(mmHg)^2}{Hz}$ in the spectrum for channel A for ascending aorta pressure.

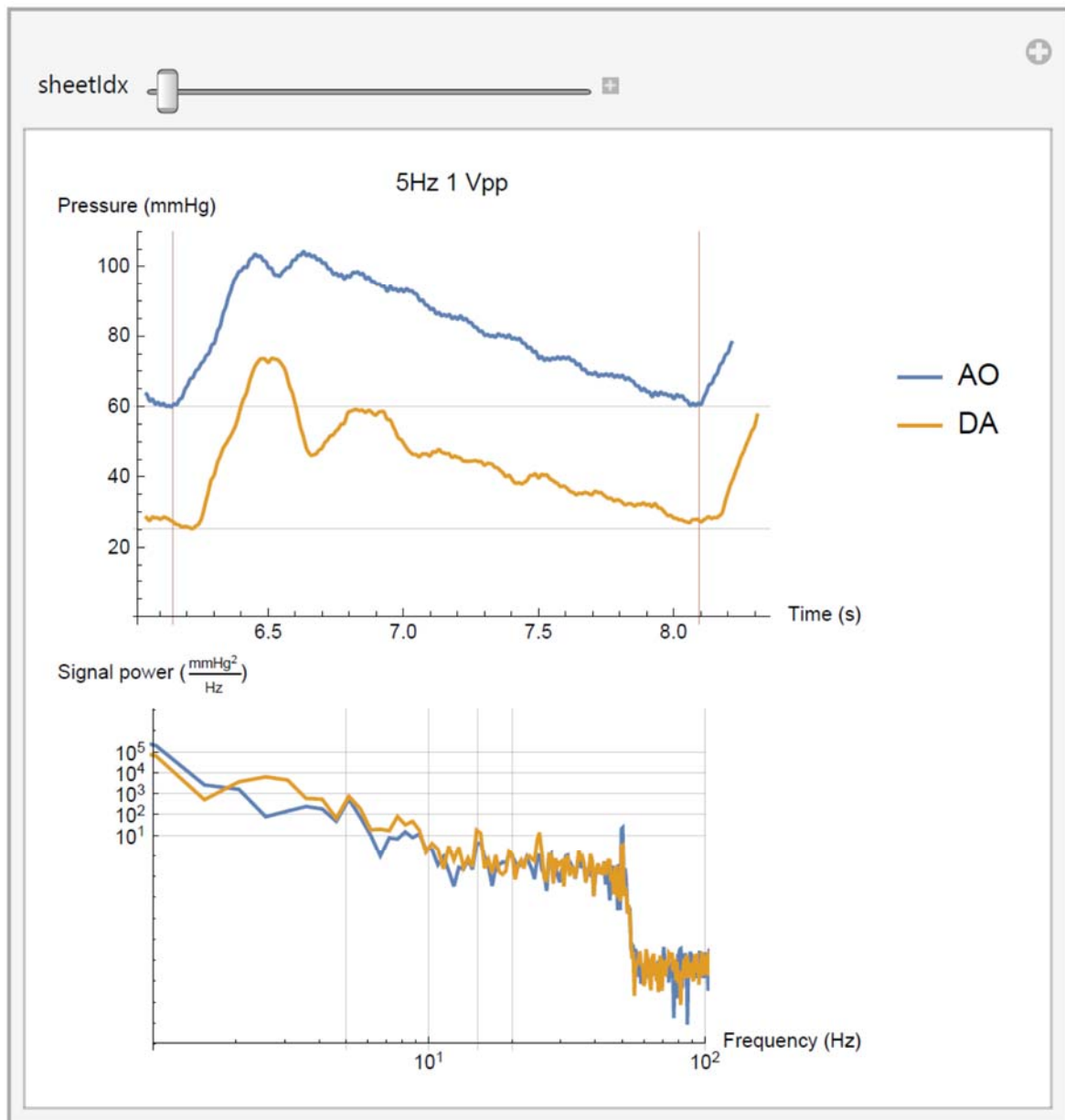


Figure 4.19: Channel A and B, Spectrum of Ascending Aorta (AO) Descending Aorta (DA) at 5 Hz and 1Vpp

The measurement shown in figure 4.19 is with the application of forced oscillations at the aorta with 5 Hz and 1Vpp. The spectra shows both ascending aorta AO and descending aorta DA, from channel A and B of the pressure waves.

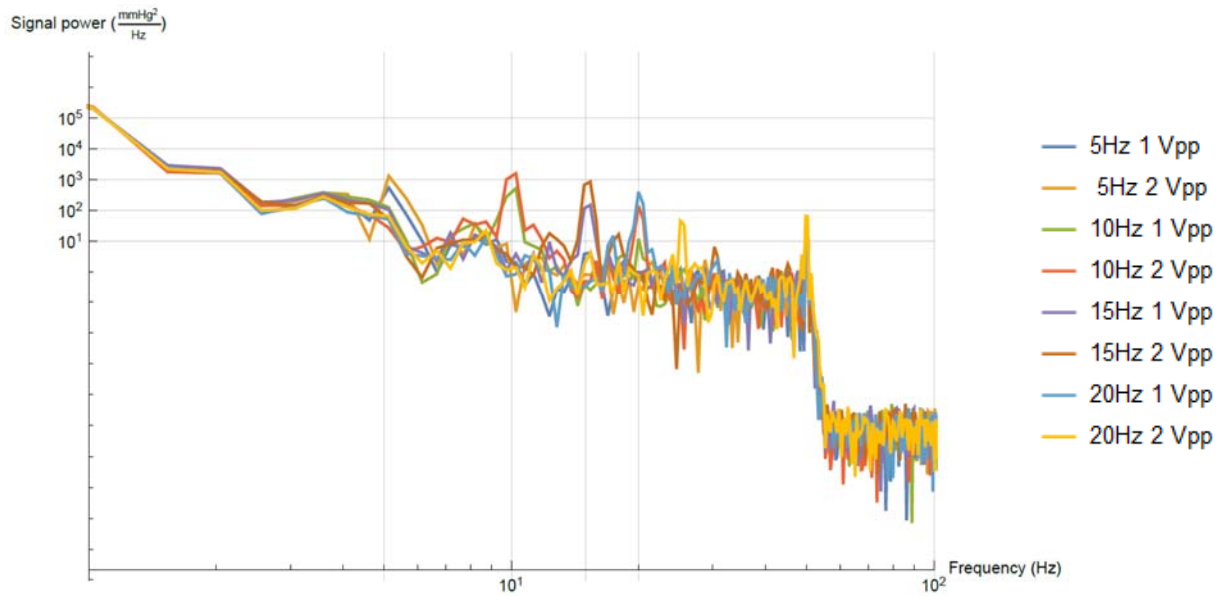


Figure 4.20: Comparison of Spectra at Channel A for Pressure wave

Figure 4.20 shows a comparison of applied forced oscillations of all applied frequencies' spectra at channel A for pressure waves at lower frequencies in Hz plotted against signal power spectral in $\frac{(mm\ Hg)^2}{Hz}$. Applied forced oscillations give a sharp rise in the signal power at lower frequencies from 5 Hz, 1 Vpp and 5 Hz till 20 Hz, 1 Vpp, and 20 Hz, 2 Vpp in the spectra.

Figure 4.21 below gives the comparisons of all applied frequencies' spectra at channel B for the pressure wave. There are few sharp changes in the power signal spectra.



Figure 4.21: Comparison of Spectra at Channel B for Pressure wave

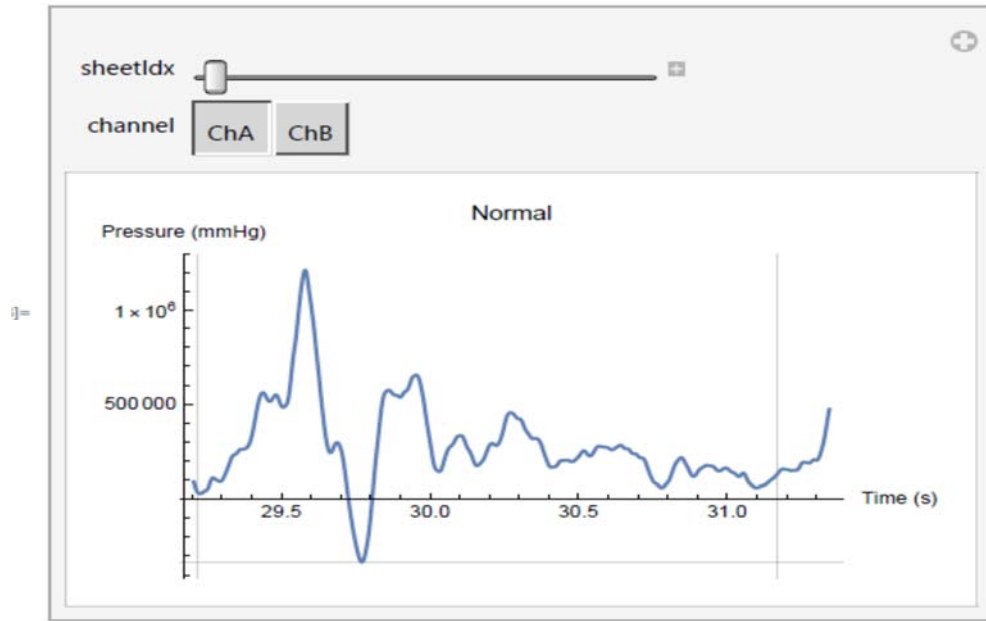


Figure 4.22: Flow Measurement Channel A

The flow measurement was carried out using the flow sensors and the phantom aorta submerged in water. Pressure in mmHg against time in seconds is shown in the above figure 4.22, whereas the comparison of flow spectra at channel A for ascending aorta is shown in figure 4.23 below, measured frequencies are in Hz versus the signal power in $\frac{(L/min)^2}{Hz}$.

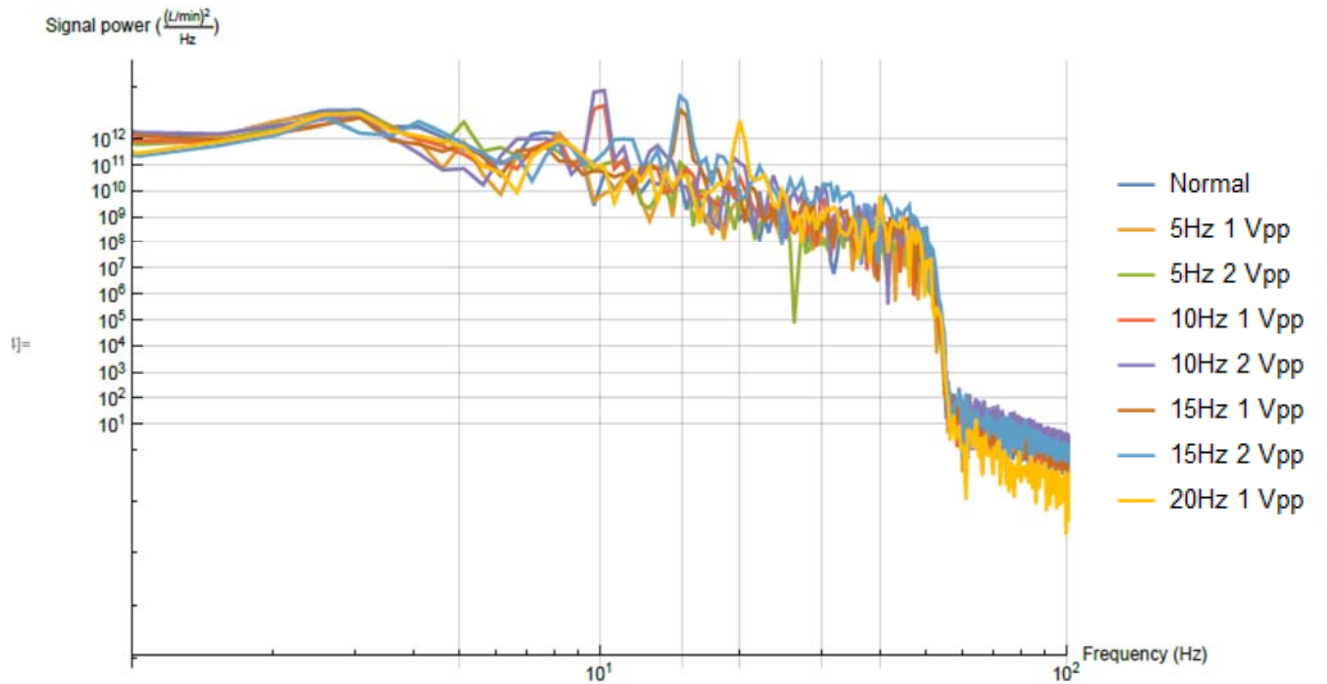


Figure 4.23: Comparisons of Flow Measurement Channel A

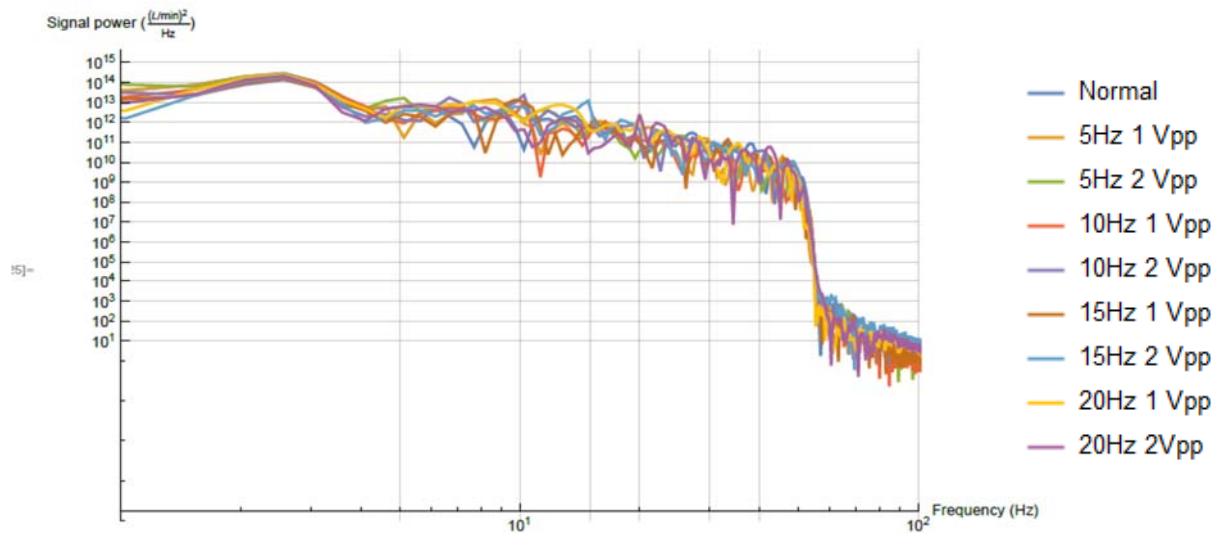


Figure 4.24: Comparison Flow Measurement Channel B

Figure 4.24 shows the comparison of flow measurement of the descending aorta at lower frequencies from 5 Hz to 20 Hz with the magnitude of 1 Vpp and 2 Vpp. The higher frequencies from 25 Hz to 49 Hz with the magnitude of 1 Vpp and 2 Vpp is taken into consideration. Observe the changes in the spectra shown in the figure 4.25 below.

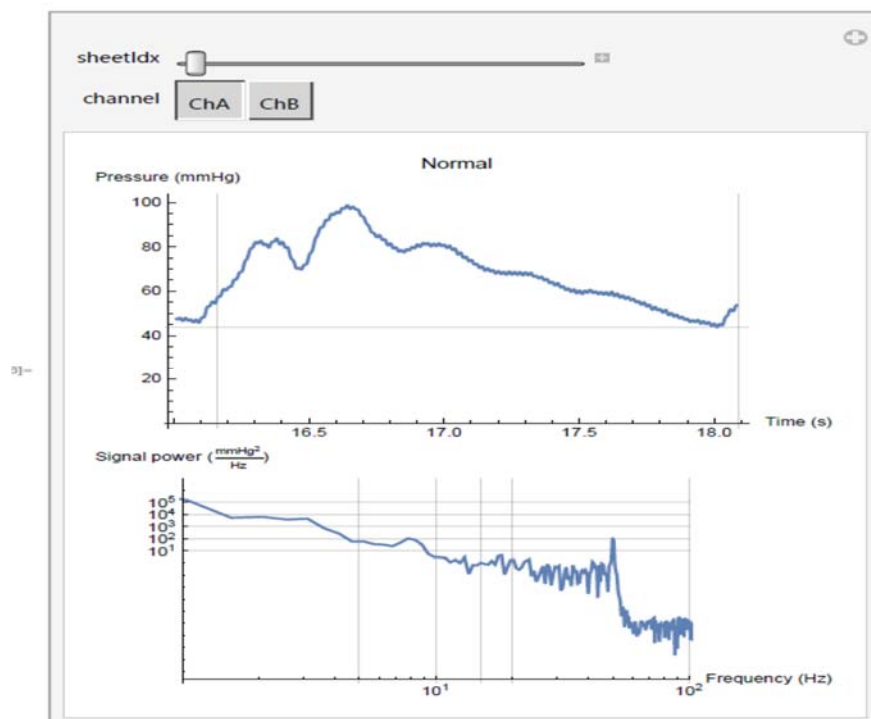


Figure 4.25: Higher Frequencies Pressure Measurement Channel A

The comparison of channel A and B spectra for both ascending and descending pressure aorta, and the normal spectra, without any frequencies applied, is shown in the figure below 4.26.

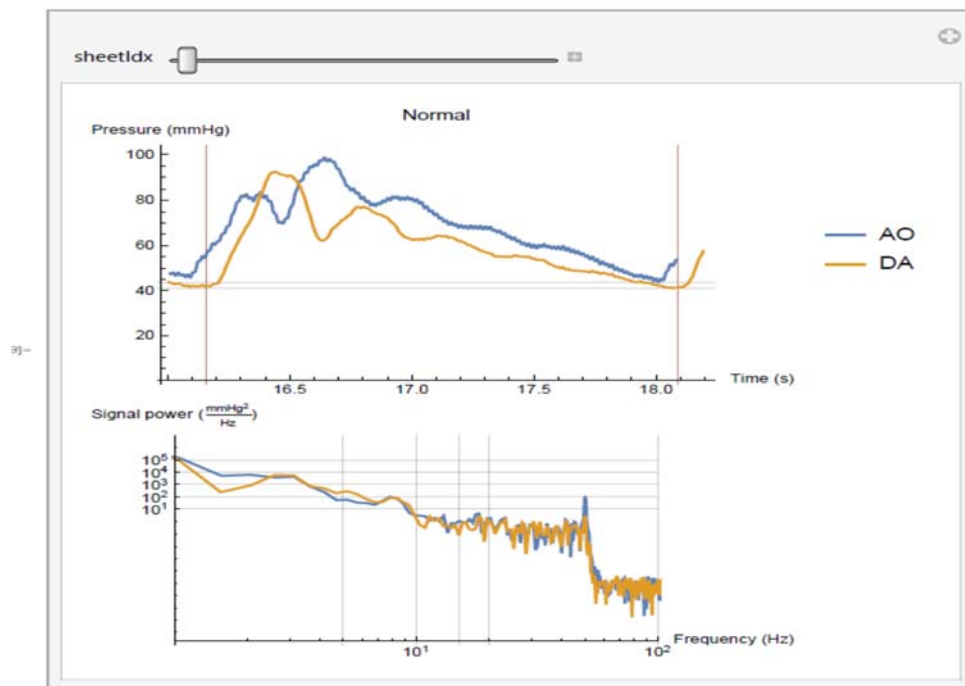


Figure 4.26: Comparison of Channel A and B for Ascending aorta (AO) and Descending Aorta (DA) Pressures

The higher frequencies pressure measurement comparison of channel A for the Ascending aorta is shown in the figure 4.27 below.

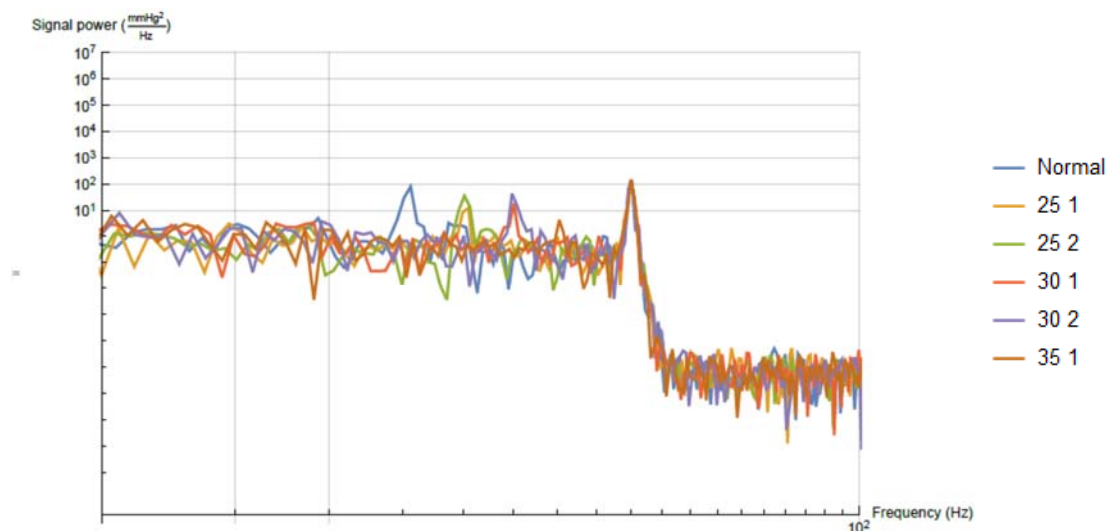


Figure 4.27: Comparison of Pressure Spectra at Channel A



Figure 4.28: Comparison of Pressure Spectra at Channel B

The results in the initial experimental setup were not giving the output response correctly due to the main factor of the transmission of the oscillation in the descending aorta point at the artificial capillary system (refer figure 3.11(b)). The descending aorta point, where forced oscillations were applied, could not hold it properly. The transmission of forced oscillation, which was directly given from the LDS[®]V406 shakers combined with function generator, was not able to penetrate properly into the aorta. This has significant impact on the output results.

The modified set up had 500 mm of length of aorta, which was submerged in fluid, along with forced displacement transducer with holding clamp at the artificial capillary system for transferring the forced oscillations signal with correct intensity. The results obtained from this set up gives a closer output to the simulation model with correct transmission of forced oscillation from descending aorta to ascending aorta for pressure and flow. The effect is noted in table 3 and 4.

4.5 Results from the final cardiovascular simulation setup

The initial modified schematic block diagram of cardiovascular simulation setup in figure 4.13 with submerged aorta in figure 4.14 and the force displacement transducer in figure 4.15, gives the new measurement readings (refer to Table 4.3). It also gives detailed information of the output which is measured from the changed experimental setup and gives a clearer spectrum

output from the system. Table 4.3 gives the readings of pressure at descending and ascending aorta, whereas table 4.4 gives the reading of descending and ascending aorta flow measurements. The LabCharts and spectrum are discussed in the discussion section of this chapter.

Table 4.3: Pressure Descending (DA) and Ascending Aorta (AO)

Input Frequencies (Hz) & Amplitude (Vpp)	Output Pressure DA mmHg	Ref Power $\frac{(mm\ Hg)^2}{Hz}$	Gain $\frac{(mm\ Hg)^2}{Hz}$	Output Pressure AO mmHg	Ref Power $\frac{(mm\ Hg)^2}{Hz}$	Gain $\frac{(mm\ Hg)^2}{Hz}$
Normal						
5 & 1	20	18	0.46	22	18	0.86
5 & 2	22	18	0.86	25	18	1.43
10 & 1	32	10	5.05	22	10	3.42
10 & 2	38	10	5.8	28	10	4.47
15 & 1	28	1.2	13.68	22	1.2	12.63
15 & 2	36	1.2	14.76	27	1.2	13.52
20 & 1	30	0.5	17.78	22	0.5	16.43
20 & 2	30	0.5	17.78	20	0.5	16.02
25 & 1	30	0.3	20.00	11	0.3	15.64
25 & 2	31	0.3	20.14	14	0.3	16.69
30 & 1	33	0.25	21.21	10	0.25	16.02
30 & 2	34	0.25	21.33	12	0.25	16.81
35 & 1	30	0.2	21.75	12	0.2	17.78
35 & 2	31	0.2	21.90	14	0.2	18.45
40 & 1	22	0.15	21.65	8	0.15	17.27
40 & 2	22	0.15	21.69	10	0.15	18.21
45 & 1	20	0.15	20.00	5	0.15	15.23
45 & 2	21	0.15	21.46	6	0.15	16.02
49 & 1	20	0.15	21.24	4	0.15	14.25
49 & 2	18	0.15	21.46	4.5	0.15	14.77

Table 4.4: Flow Descending (DA) and Ascending Aorta (AO)

Input Frequencies (Hz) & Amplitude (Vpp)	Output Flow $\frac{(L/min)^2}{Hz}$	Ref Power $\frac{(L/min)^2}{Hz}$	Gain $\frac{(L/min)^2}{Hz}$	Output Flow AO $\frac{(L/min)^2}{Hz}$	Ref Power $\frac{(L/min)^2}{Hz}$	Gain $\frac{(L/min)^2}{Hz}$
Normal						
5 & 1	122	120	0.071	123	120	0.10
5 & 2	121	120	0.036	122	120	0.071
10 & 1	132	110	0.79	122	110	0.45
10 & 2	135	110	0.89	132	110	0.79
15 & 1	126	102	0.92	120	102	0.70
15 & 2	132	102	1.12	122	102	0.78
20 & 1	121	100	0.83	122	100	0.86
20 & 2	124	100	0.93	123	100	0.90

The comparison of pressure gain spectra with different voltage and frequencies and at different locations is given in the figures 4.29, 4.30 and 4.31 given below to complement table 4.3

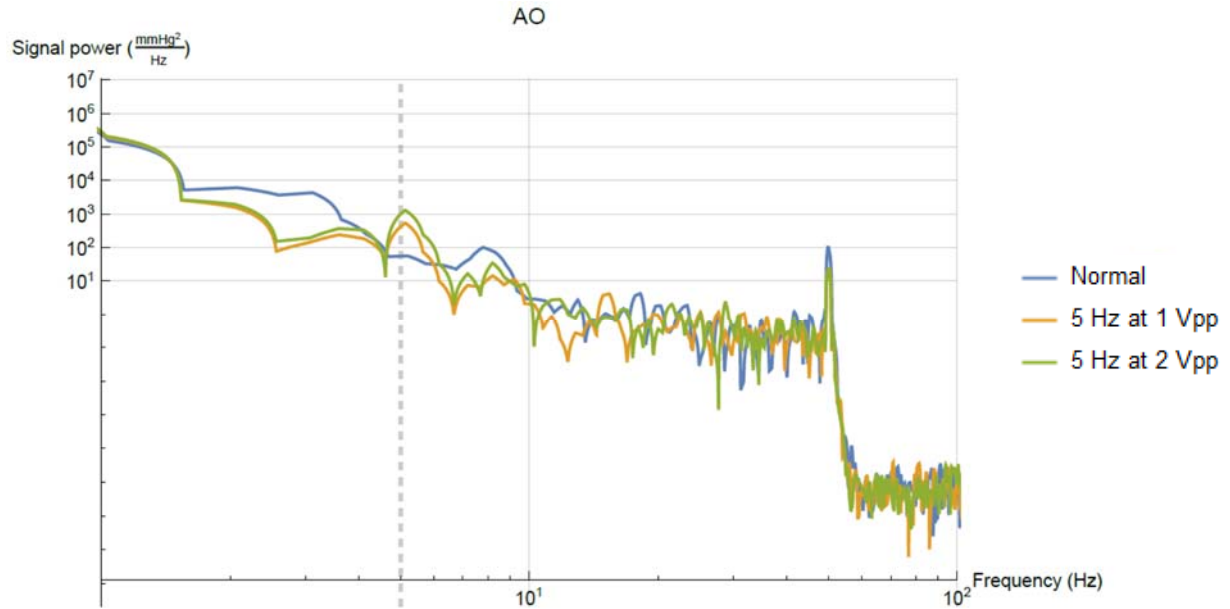


Figure 4.29: Comparison of pressure gain spectra at different voltages

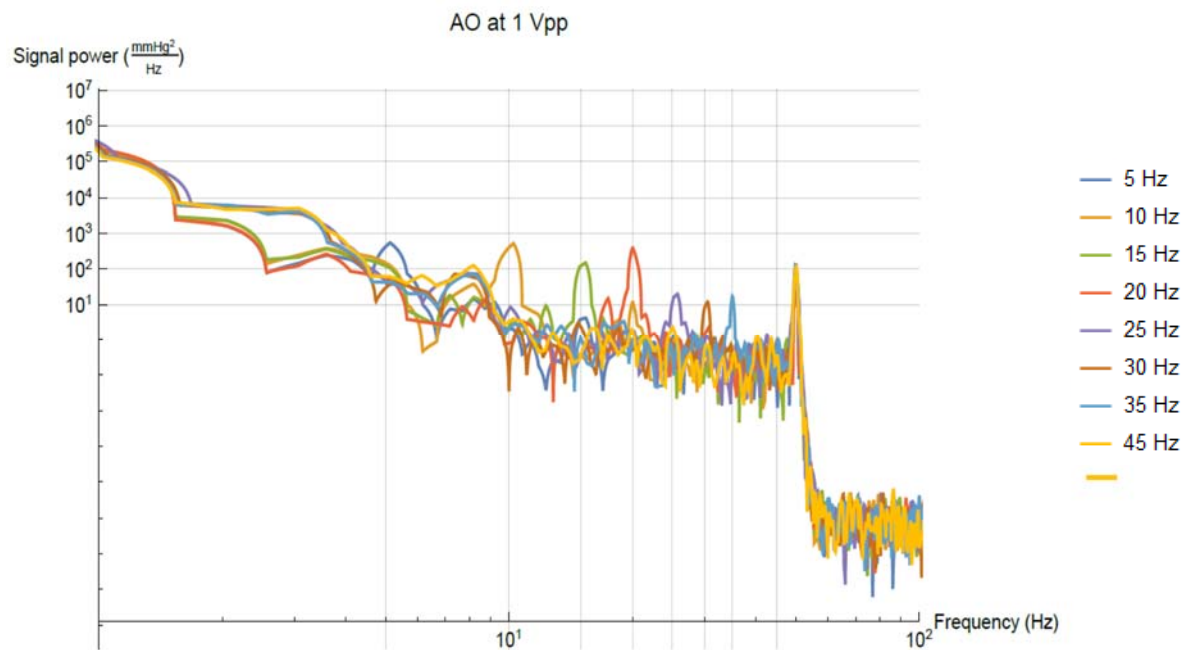


Figure 4.30: Comparison of pressure gain spectra at different frequencies

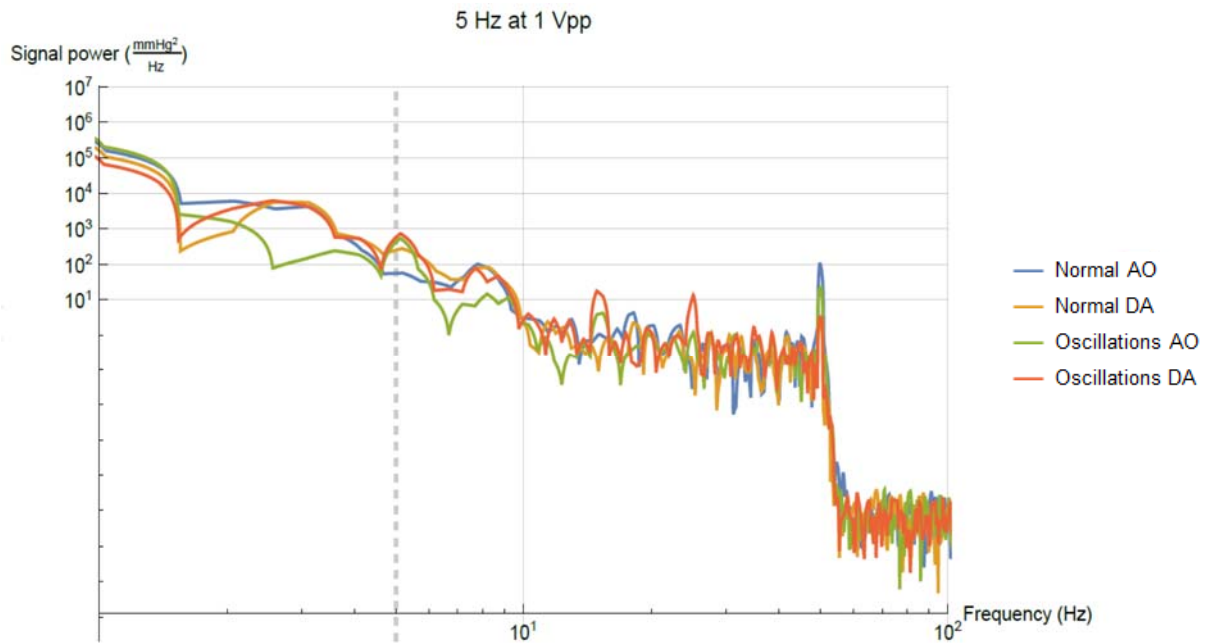


Figure 4.31: Comparison of pressure gain spectra at different locations

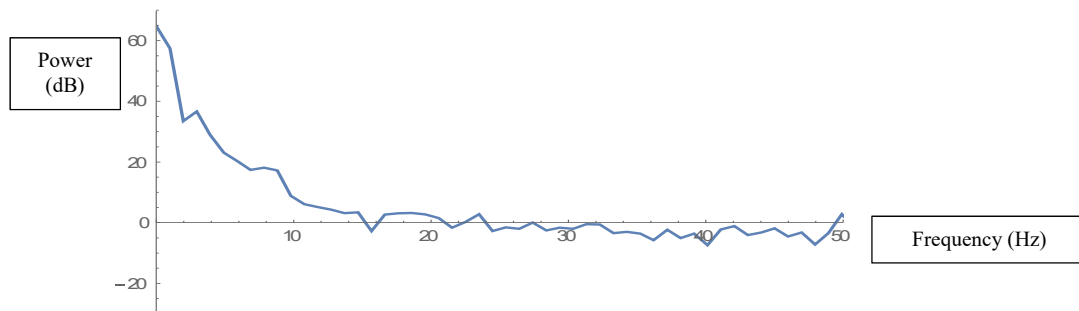


Figure 4.32: New Experimental Setup Normal Spectrum of Pressure- Descending Aorta (Phantom) without forced oscillation

Figure 4.32 shows the spectrum output of the pressure of the phantom for descending and ascending aorta without any forced oscillation. This first normal spectrum used to start the spectrum analysis is the reference point for the subsequent applied frequencies of 5Hz, 10Hz, 15Hz, 20Hz, 25Hz, 30Hz, 35Hz, 40Hz, 45Hz and 49Hz with each frequency along with 1Vpp and 2Vpp amplitude application from the function generator of the sinewave as forced oscillation. Table 4.3 is the spectrum output of signal based on the frequencies and voltages mentioned above to obtain the output signal for this research. The Table 4.3 is the spectrum for both pressure values of descending and ascending aorta.

On a similar note to the pressure gain mentioned above, the flow gain is shown in figures 4.32, 4.33 and 4.34 at different voltages, frequencies and locations to complement the table 4.4 for flow.

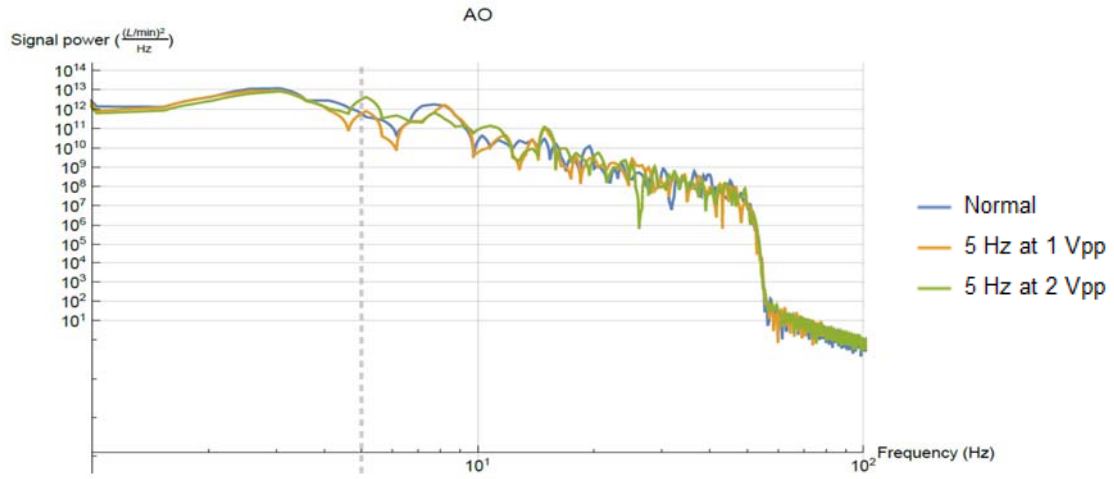


Figure 4.33: Comparison of flow gain spectra at different voltages

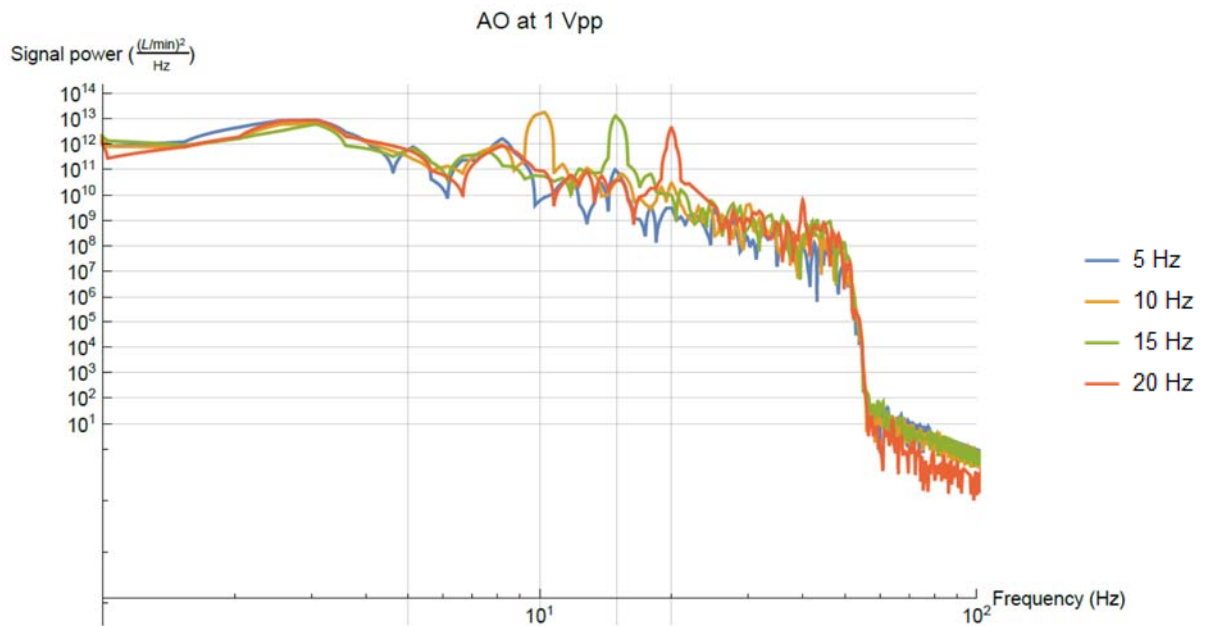


Figure 4.34: Comparison of flow gain spectra at different frequencies

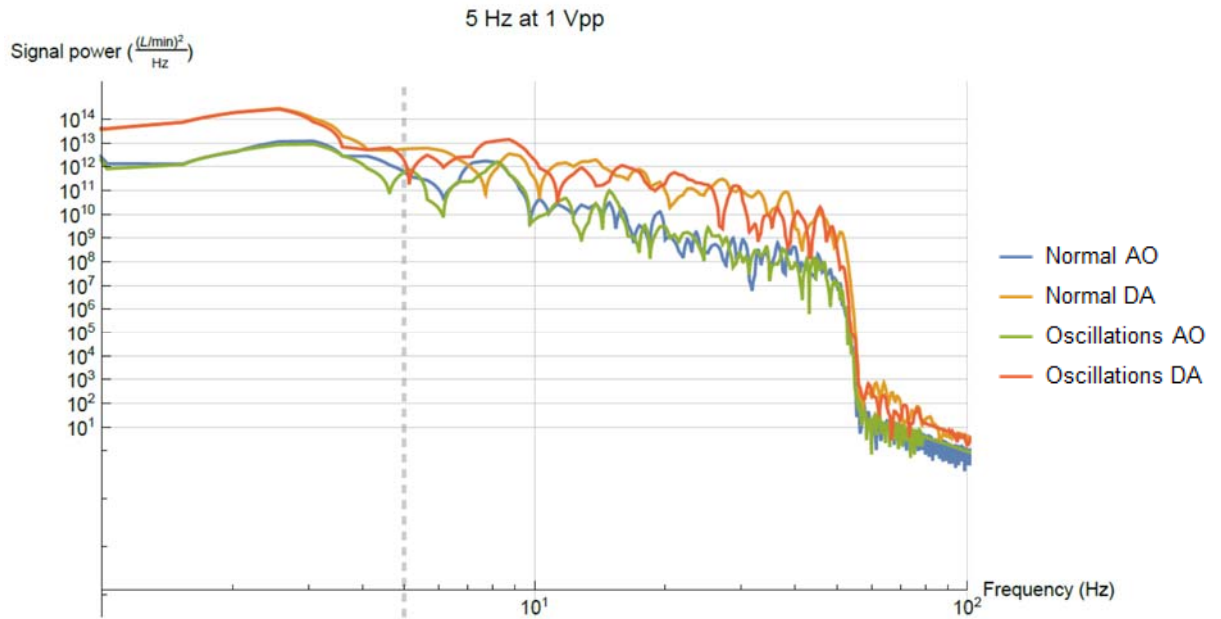


Figure 4.35: Comparison of flow gain spectra at different locations

The forced oscillations applied at various frequencies to the phantom aorta were then validated by applying in the simulation to verify the application responses. Table 4.3 shows the main output results to validate both the simulated and the experimental results. It begins with the application of the sine wave of 5Hz frequency and 1 Vpp and then 2 Vpp at very low frequency. There was little change in the power signal gain output whereas as the frequency increased there is significant change in the output response especially at the frequencies of 30 Hz and 35 Hz which is also very important for smooth airwave tissues [16-18].

Details about the output spectrum of the ascending aorta from the experimental set up applied to the simulated model both gave approximately the correct output. This has validated both the simulated and the experimental set up. It worked effectively to give the output response of pressure and flow to the changes in the application of the forced oscillations applied at different frequencies and at different magnitude.

Chapter 5: Discussion on the Analysis of the Simulation and Experimentation results

5.1 Introduction

This chapter is devoted to the detailed discussions on both analysis of simulation results and the experimental results with comparison. It starts with the results from the simulation output and then subsequently goes into the experimental output results, keeping in mind the research objectives.

5.2 Discussion of Simulation and Experimental results

The Salient features of both Simulation and experimental Results

It was expected that the first prototype simulated model should respond to the applied signal, but it did not happen.

Similar things happened with the experimental analysis as it did not respond the way it was expected with many issues encountered on the journey to get desired output.

The simulated models were required to respond to the various types of signals like exponential, impulse etc. The later simulated models were more refined with the use of the correct curve fitting interpolation and a representative heart beat to give a final corrected simulated model. This played a very important role to get final output from the simulation model of this research.

On the other hand, the initial experimental set up did not give the response expected. It was mainly due to the incorrect holding of the artificial capillary system at the point of the applied forced oscillation signal to descending aorta. The previous research group's experimental development of the phantom model mechanism was developed according to their requirements. It was immediately noted that a workable solution was needed to fix up the gap with changing the length of the aorta, introduction of force displacement transducer and correct clamp holder for artificial capillary system for this research work.

The new modified experimental setup, in the previous chapter, provides the output which is the backbone of this research. In the new modified experimental set up, to get the proper transmission of the applied forced oscillation, a force transducer was introduced in between the LDS shaker and capillary holder at the Descending Aorta. This set up has changed the output response signal significantly (refer below the spectra of the experimental analysis of various applied frequencies to the Descending Aorta and corresponding response at the Ascending Aorta) which is the main objective of this research.

Firstly, let us discuss the descending aorta spectrum, as this is the point where we have applied our forced oscillation signal to see the response both at descending aorta in LabChart as well as in the simulated model where it was applied from the output response collected from the experimental set up.

Table 5.1: Descending Aorta Pressure output from 25 Hz to 35 Hz under different amplitudes

Input Frequencies (Hz) & Amplitude (Vpp)	Output Pressure DA mmHg	Ref Power $\frac{(mm\ Hg)^2}{Hz}$	Gain $\frac{(mm\ Hg)^2}{Hz}$
25 & 1	30	0.3	20.00
25 & 2	31	0.3	20.14
30 & 1	33	0.25	21.21
30 & 2	34	0.25	21.33
35 & 1	30	0.2	21.75
35 & 2	31	0.2	21.90

As it is evident from table 4, there is a significant change in the output response of the descending aorta output pressure. The amplitude plays a very important role along with the frequency. The relative gain is always increasing at higher value of amplitude with the same frequency. As the frequencies increases from 40 Hz to 49 Hz the response started reducing and did not show any changes, irrespective of the amplitude increment in the oscillations. Also, during the experimental testing, it has been observed that the magnitude higher than the 2 Vpp oscillates drastically which makes the entire experimental set up shake and become too unstable to take further measurement. This is one of the limitations for this research. Also, the Power amplifier gain for the LDS shaker is to be kept below half, as this also has an effect on the oscillation intensity due to the shaking of the shaker at very high speed. As the descending aorta is the point of application of the forced oscillation, due to decrease in the diameter, the response was very fast, whereas the response of the ascending aorta, due to forced oscillations

applied at the descending aorta, is slightly different. This will be shown subsequently with the discussion about the output response of the ascending aorta.

It is evident from the results section of the previous chapter, from figures 4.18 to 4.36, that the spectrum output responses show the changes observed from the applications of various frequencies and the corresponding amplitude. This information about the responses from the new experimental set up was validated by the simulated model. However, there are significant differences in the output response of the ascending aorta blood pressure compared to the descending aorta blood pressure (refer table 5.2 in the next paragraph).

Table 5.2: Comparison of DA and AO Pressure output from 25 Hz to 35 Hz

Input Frequencies (Hz) & Amplitude (Vpp)	Output Pressure DA $(mm\ Hg)^2$ Hz	Ref Power $(mm\ Hg)^2$	Gain $(mm\ Hg)^2$	Output Flow AO $(mm\ Hg)^2$ Hz	Ref Power $(mm\ Hg)^2$	Gain $(mm\ Hg)^2$
		Hz	Hz		Hz	Hz
25 & 1	30	0.3	20.00	10	0.3	15.22
25 & 2	31	0.3	20.14	10.5	0.3	15.44
30 & 1	33	0.25	21.21	10	0.25	16.02
30 & 2	34	0.25	21.33	12	0.25	16.81
35 & 1	30	0.2	21.75	12	0.2	17.78
35 & 2	31	0.2	21.90	14	0.2	18.45

Table 5.2 shows the comparison between both the spectrum response of the descending and ascending aorta under the influence of forced oscillations from frequencies from 25 Hz to 35 Hz with 1 Vpp and 2 Vpp. These frequencies give significant changes in the output responses to the blood pressure of both descending and ascending phantom aorta of the human in the modified experimental set up.

The comparisons gives us very interesting point about the output responses of the phantom aorta of the human. There is a significant change in both descending and ascending aorta and they do differ in their output power magnitude and relative gain. The absolute pressure of the ascending aorta (AO) is lower (see table 5.2) than for the descending aorta (DA). The pressure gain is smaller for the lower frequency of 5 Hz as compared to higher frequencies according to “aortic pressure” in channel A, this is mainly due to signal strength transmission at low frequencies.

The reason is that the oscillations at higher frequencies and amplitudes above 2 Vpp create instability in the experimental set up; also self-vibration of aorta may reduce the magnitude of

pressure and flow. The flow or discharge rate (Q) at low frequencies in both channels A and B has a roll-off magnitude of power steeper than for pressure. This is due to the response of the flow sensors sensitivity. Also, interestingly, in channel B the peaks do not rise far above the noise floor this is because of the application of forced oscillations is at descending aorta, which has low noise from the force displacement transducer. The peaks of pressure in channel B at higher frequencies is much clearer than the peaks of pressure in channel A at higher frequencies and this is due to transmission losses from descending aorta to ascending aorta.

The difference between 1 Vpp and 2 Vpp of applied amplitude is quite small but they are consistent $2 > 1$, this is due to stable function generator and stable clamp holder for transmitting the signal to descending aorta. The pressure attenuation is different than flow (Q) from descending to ascending aorta, mainly due to different sensing devices for pressure and flow, the surrounding conditions and transmission of signal. Although, according to simulation there should be almost no attenuation, the simulation is software-based that has all the parameters set in the coding with ideal conditions. The magnitudes are low for normal and oscillating AO as compared to normal and oscillating DA, over all frequencies. This is because in the experimental set up the DA is receiving forced oscillations first as compared to AO, hence the difference is due to very small delay in the signal to reach AO and also some losses in the transmission. Please refer to appendix F for all the spectrum output results for both pressure and flow at AO and DA.

We can see from the table 5.1, that both the descending and ascending blood pressure output and relative gain in $\frac{(mm\ Hg)^2}{Hz}$ show significant increase in the frequencies of 30 Hz and 35 Hz and in the 2 Vpp magnitude of the sinusoidal signal applied as forced oscillations from the function generator. Both descending and ascending aorta measurement were taken at the same time and the same has been recorded instantaneously through LabChart. Another important aspect to be noticed was that the measurement shows that the descending aorta response is much higher for the pressure output whereas the relative gain is reasonably higher than the ascending aorta. Note the comparison in table 5.3 of the blood flow for descending and ascending aorta.

Table 5.3: Comparison of Descending and Ascending Aorta Flow measurement

Input Frequencies (Hz) & Amplitude (Vpp)	Output Flow DA (L/min) $\frac{L/min}{Hz}$	Ref Power (L/min) ² $\frac{(L/min)^2}{Hz}$	Gain (L/min) ² $\frac{(L/min)^2}{Hz}$	Output Flow AO (L/min) ² $\frac{(L/min)^2}{Hz}$	Ref Power (L/min) ² $\frac{(L/min)^2}{Hz}$	Gain (L/min) ² $\frac{(L/min)^2}{Hz}$
Normal						
5 & 1	122	120	0.071	123	120	0.10
5 & 2	121	120	0.036	122	120	0.071
10 & 1	132	110	0.79	122	110	0.45
10 & 2	135	110	0.89	132	110	0.79
15 & 1	126	102	0.92	120	102	0.70
15 & 2	132	102	1.12	122	102	0.78
20 & 1	121	100	0.83	122	100	0.86
20 & 2	124	100	0.93	123	100	0.90

Referring to table 5.2 above, blood flow output response measured values at 10 Hz and amplitude 2 Vpp gives the highest output flow in descending aorta and the same is true for the ascending value, but with marginally less value for the relative gain in the ascending aorta. The relative gain at 15 Hz and 2 Vpp gives the highest value for the descending aorta. Another noteworthy observation is that unlike blood pressure values in both descending and ascending aorta the blood flow shows very marginal differences in terms of blood flow and their corresponding values of relative gain in the spectrum which means forced oscillations do not have significant impact on blood flow. However, an important limitation observed for the flow measurement for both descending and ascending aorta is that at higher frequencies from 25 Hz onwards the submerged aorta (refer figure 4.17 in the previous chapter) does not show any significant changes at both the amplitudes of applied forced oscillations. Hence the experimental values were measured up to 20 Hz and 2 Vpp.

The factors which may be responsible for the changes would be the following;

- Distance of the point of application of the forced oscillation: the descending aorta is very near to the point of forced oscillations. Due to this reason it has more impact on the both pressure measurement and the relative gain of the output responses.
- Strength of the signal applied plays a very important role in the output response. For the present measurement there was a restriction on the magnitude of applied forced oscillations. As the magnitude of the amplitude of the signal increases more than 2 Vpp the entire set up was vibrating and shaking which was disturbing the experimental set

up. This is one of the important limitation encountered during the experimental measurement of the forced oscillations to the phantom aorta of human.

- (c) The transmission of the forced oscillations has to travel a certain distance from the descending aorta to ascending aorta which results in reduction of the output response for pressure output while flow has no impact, whereas the simulation does not show any reduction.
- (d) Another important factor is the diameter of the descending aorta. As the diameter decreases towards the descending aorta, this results in higher contraction and relaxation effects on the aortic wall and its tissues and also the pressure at the descending aorta is slightly higher, whereas diameter at the ascending side is increasing and due to this pressure decreases and has less effects on the contraction and relaxation on the aortic wall and its tissues.
- (e) The thickness of the aortic wall was constant. The slight variation in the thickness will affect the measurement
- (f) Only Dragon Skin[®] 10 material used for the construction of the phantom aorta. Other materials may have significant impact on the measured values

5.3 Final comments

As seen from the above discussion on the simulation and the experimental analysis of the response of the forced oscillation on the phantom aorta, both descending and ascending aorta pressure and flow were measured and they were validated through the experimental analysis with the simulated values. There were definitely many changes required in both simulation as well as in the modified experimental set up. The output gave many important points which can take this research to the next level which will be discussed in the final conclusion chapter.

Chapter 6: Conclusion and future scope

6.1 Conclusion

The main objectives of this research work was to study the effect of induced/forced oscillations to simulate the normal human aorta by using a phantom aorta model through the application of forced oscillation at the descending aorta. Once achieved, an analysis was completed on the response of the pressure and flow, due to pulsating nature of the blood at both descending and ascending aorta, and its impact on the aortic tissue. The forced oscillations were applied at various frequencies starting from 5 Hz to 49 Hz as this is the range used in previous work at the IBTec for the respiration. Two amplitudes applied to the forced/induced oscillations from the function generator along with pulsatile blood flow were examined and the results were recorded. The results obtained were noteworthy and gave important observations which will be very useful for the future works in this area. Specifically, a very distinct observation is that significant change in the measured pressure in response to forced oscillations occurred for the frequency range between 30 Hz and 35 Hz with maximum amplitude of 2 Vpp. The results showed a significant increment in the pressure and also relative gain of the output in the power spectrum. The inference can be drawn that at the point of application of forced oscillations at the descending aorta the response shows significant increase in the measure value. However, the ascending aorta shows reduced gains under the same conditions when measured simultaneously. It is important to note that responses below 30 Hz (5 to 25 Hz) and above 35 Hz (40 Hz to 49 Hz) gave lesser pressure response, whereas flow, on the contrary, gave results mostly in the lower frequencies (5 Hz to 20 Hz) of applied forced oscillations. This implies that the applied forced oscillation responds well between 30 Hz to 35 Hz with maximum amplitude up to 2 Vpp, while flow has very weak response between 5 Hz to 20 Hz only. The application of higher frequencies to the fluid carrying submerged aorta did not respond (table 4.3 and 4.4 from chapter 4).

This research work is an extension in airway smooth muscle to a study of aortic tissue, and the phenomena that induce oscillations in the aorta modelled as a fluid-conveying pipe with change diameter. The simulated modelling were successfully achieved through the use of Mathematica 10 software.

There were a few limitations associated with the measurements during the simulation and experimentation analysis for both pressure as well as flow in the phantom aorta:

- (a) The forced oscillation signal amplitude cannot be applied at more than 2 Vpp for the pressure measurement, as this will induced uncontrollable oscillations which has the strong tendency to disturb the entire experimental set up which makes it impossible take the readings.
- (b) The flow measurement does not respond at the higher frequencies.
- (c) This research work was carried out using a phantom aorta and it is not real human aorta.
- (d) Only Dragon Skin 10 was used and no other materials were used

6.2 Future Scope

There are many experimental refinement techniques needed to get closer to the human aorta output response. There is a need for refinement to measure at higher amplitude for blood pressure measurements and for higher frequencies in the flow measurement.

Due to the pulsating nature of the blood, the impact of the higher frequencies and amplitude of the forced oscillation can be studied to give more detailed analysis on the effects of the pressure and flow in the aorta. Further research in the aortic tissues response, during the application of the forced oscillations is needed to develop greater understanding of the vibrations in the aorta itself. The self-vibration or oscillations of the aorta can be studied in more detail in order to get more information about the nature of aortic tissues.

The validation can be done on animal tissues and then on human tissues to compare and check the contraction and relaxation phenomenon. Further future development is also desirable for the creation of other materials to be manufactured that are closer to the original, in anticipation of more accurate results.

Appendix A: Simulation Coding of Mathematica for mathematical model

```

PWV[r_,h_,Y_,ρ_]:=Sqrt[(Y h)/(ρ r)]
SegmentPV [r_, h_, Y_, ρ_, θ_, x_, t_,p_,v_, xStart_, dx_, pxStart_,
vxStart_, fext_]:=Module[{A, k, c, pde, g=9.81, pvSolution},
  c=PWV[r,h,Y,ρ];
  PrintTemporary[c];
  PrintTemporary[r];
  PrintTemporary [fext];
  A=π r2;
  k=A/(ρ c2);
  pde={- k D[p[x,t],t]==A D[v[x,t],x],fext/A-A g Sin[θ]-D[p[x,t],x]== ρ
D[v[x,t],t],
      p[xStart,t]==pxStart,v[xStart,t]==vxStart,
p[x,0]==(pxStart/.t-> 0), v[x,0]==(vxStart/. t-> 0)};
  pvSolution=NDSolve[pde,{p[x,t],v[x,t]},{x,xStart,xStart+dx},{t,0,3}];
  pvSolution[[1]]
]

xStep=0.04/4;
nStep=10*4;
r=0.0107;
dr=0.00055/nStep;
R=0.1;
pvs=ConstantArray[Missing[], nStep];
pxStart=pinterpd[t];(*FourierSinSeries[8t,t,6]*);
vxStart=pxStart/((1+R)*1050*PWV[r, 0.73, 130000,1050]/(1-R));
xfext=0.25 Sin[8 t];
Do[
  PrintTemporary[n];
  pvs[[n]]=SegmentPV[r, 0.73, 130000, 1050, 0, x,t,p,v, (n-1) xStep, xStep,
pxStart,vxStart,If[n==1,xfext,0]];
  pxStart=(p[x,t]/. pvs[[n]])/.x-> n xStep;
  vxStartOld=(v[x,t]/. pvs[[n]])/. x-> n xStep;
  vxStart=vxStartOld*(r/(r+dr))2;
  (*vxStart=(v[x,t]/. pvs[[n]])/. x□ n xStep;*(r/(r+dr))2*)
  r=r+dr;
  ,{n,nStep}
]

pTable=Flatten[Table[{x,t,p[x,t]/.pvs[[n]]}, {n,1, nStep,1},{x, (n-1)xStep,
n xStep, 0.01}, {t, 0,3, 0.01}],2];
ListPlot3D[pTable]
vTable=Flatten[Table[{x,t,v[x,t]/.pvs[[n]]}, {n,1, nStep,1},{x, (n-1)xStep,
n xStep, 0.01}, {t, 0,3, 0.01}],2];
ListPlot3D[vTable]

sine wave

```

```

{- k D[p[x,t],t]==A D[v[x,t],x],
  f_external/A[t]-A g Sin[θ]-D[p[x,t],x]== ρ D[v[x,t],t],
p[0.004,t]==p01,v[0.004,t]==v01} /. {A[t]->A,k->A/(ρ c^2)} (*j[t]□pc
Abs[cA]/(2DA)*)
%/. {h->0.0066,r->0.0142,ρ->1050,A->π/4 (2r)^2,c->4.468, f_external->0.0000
Sin[12π t],θ->0,g->9.81}
s= NDSolve[%,{p[x,t],v[x,t]},{x,0.004,.008},{t,0,3}]
Plot3D[p[x,t]/.%, {x, 0.004,0.008}, {t, 0,3}]

Beat

data0219=Import["E:\\Data from Shaker taken on 02 Feb17.xlsx"]

sheet=1;
data0219ch1=data0219[[sheet,10;;-1,{5,6}]]/. ""->Missing[];
fs=1/(data0219ch1[[2,1]]-data0219ch1[[1,1]]);
ListLinePlot[data0219ch1,GridLines-
>{Automatic,{Min[DeleteMissing@data0219ch1[[All,2]]]}}]

beatRange=<|1->Interval[{7.20,9.66}],2->Interval[{4.98,7.43}],7-
>Interval[{48.13,50.58}],8->Interval[{7.12,9.8}]]>
beat0219ch1=Select[data0219ch1,IntervalMemberQ[beatRange[sheet],#[[1]]]&];
ListLinePlot[beat0219ch1,GridLines-
>{Automatic,{beat0219ch1[[1,2]],beat0219ch1[[-1,2]]}}]

psd={Subdivide[0,fs,Length[beat0219ch1]-
1],PeriodogramArray[beat0219ch1[[All,2]]]}□;

Interpolation
pinterpd=Interpolation[book1p,Method- "Spline", InterpolationOrder->2]
pEvenlySampled = Table[pinterpd[t], {t,Min[book1p[[All, 1]]],
Max[book1p[[All, 1]]], 0.03} ];
pinterpd = ListInterpolation[ pEvenlySampled~Prepend~pEvenlySampled[[-1]],
{{0, 0.6}},
PeriodicInterpolation -> True]
Plot[pinterpd[t], {t, 0, 1.6}, AspectRatio -> 1/3, ImageSize -> Large,
PlotPoints -> 1000]

```


Appendix B: Smart Motor programming code

```
EIGN(W,0)
ZS
CTE (1)
CTA (23,100)
CTW (0)
CTW (2664)
CTW (4995)
CTW (6993)
CTW (8658)
CTW (9990)
CTW (10822)
CTW (11389)
CTW (11655)
CTW (9000)
CTW (7500)
CTW (6000)
CTW (4500)
CTW (3500)
CTW (2400)
CTW (1600)
CTW (1100)
CTW (700)
CTW (400)
CTW (150)
CTW (75)
CTW (40)
CTW (0)
SRC (2)
MCE (2)
MCW (1,0)
MC
MCMUL = 2
MCDIV = 1
MFMUL = 1
MFDIV = 7
MFA (0)
MFD (0)
MFSDC (0,0)
G
END
```

Appendix C: LDS Shaker 405 and LDS® PA 100E power amplifier

Permanent Magnet Shakers



left to right: V100 Series, V200 Series on trunnions, V200 Series, V400 Series, V400 Series on trunnions, V450 Series on trunnions, V450 Series

LDS Shaker Model	V100 Series	V200 Series	V400 Series	V450 Series	V455 Series
Recommended LDS Amplifier	LPA100	LPA100	LPA100 - no fan LPA600 - with fan	LPA600	LPA1000
Natural Air Cooling (no fan)					
Sine Peak Force	8.9 N (2.0 lbf)	17.8 N (4.0 lbf)	98.0 N (22.0 lbf)	177.0 N (39.8 lbf)	—
Random Force rms	—	—	38.0 N (8.5 lbf)	—	—
Half-sine Shock Force†	—	—	90.0 N (21.0 lbf)	—	—
Velocity Sine Peak	1.31 m/s (51.6 in/s)	1.49 m/s (58.7 in/s)	1.52 m/s (59.8 in/s)	1.78 m/s (70.1 in/s)	—
Acceleration Sine Peak	1373 m/s ² (140.0 g _n)	892 m/s ² (91.0 g _n)	490 m/s ² (50.0 g _n)	415 m/s ² (42.3 g _n)	—
Acceleration Random rms	—	—	190 m/s ² (19.4 g _n)	—	—
Displacement Peak-Peak‡	2.5 mm (0.1 in)	5.0 mm (0.2 in)	14.0 mm (0.55 in)	19.0 mm (0.75 in)	—
Forced Air Cooling (with fan)					
Sine Peak Force	—	—	196 N (44.0 lbf)	311 N (70.0 lbf)	489 N (110.0 lbf)
Random Force rms	—	—	89 N (20.0 lbf)	214 N (48.0 lbf)	290 N (66.0 lbf)
Half-sine Shock Force*	—	—	200 N (44.0 lbf)	460 N (103.0 lbf)	730 N (163.0 lbf)
Velocity Sine Peak	—	—	1.78 m/s (70.1 in/s)	1.78 m/s (70.1 in/s)	2.50 m/s (98.4 in/s)
Acceleration Sine Peak	—	—	980 m/s ² (100.0 g _n)	730 m/s ² (74.4 g _n)	1147 m/s ² (117.0 g _n)
Acceleration Random rms	—	—	446 m/s ² (45.5 g _n)	501 m/s ² (51.1 g _n)	686 m/s ² (70.0 g _n)
Displacement Peak-Peak‡	—	—	17.6 mm (0.69 in)	19.0 mm (0.75 in)	—
Mass of Moving Elements	0.0065 kg (0.014 lb)	0.02 kg (0.044 lb)	0.2 kg (0.44 lb)	0.426 kg (0.94 lb)	—
Body Mass – base mounted	0.91 kg (2.0 lb)	1.81 kg (4.0 lb)	14.1 kg (31.0 lb)	64.0 kg (141.1 lb)	—
Body Mass – trunnion mounted	—	3.17 kg (7.0 lb)	22.7 kg (50.0 lb)	81.7 kg (180.1 lb)	—
Armature Resonance (f _n)	12000 Hz	13000 Hz	9000 Hz	6000 Hz	—
Usable Frequency Range	dc to 12000 Hz	dc to 13000 Hz	dc to 9000 Hz	dc to 7500 Hz	—
Acoustic Noise‡					
Shaker naturally cooled	< 70 dBA	75 dBA	82 dBA	105 dBA	—
Shaker forced-air cooled	—	75 dBA	105 dBA	105 dBA	—
Total Heat Dissipation	9.5 W	48.0 W	340 W	820 W	1.6 kW
Max. Ambient Working Temperature	30 °C (86 °F)				
Maximum Dimensions Base-mounted shaker	89.0 x DIA 65.0 mm (3.5 x DIA 2.6 in)	96.0 x DIA 78.0 mm (3.8 x DIA 3.1 in)	198.4 x DIA 165 mm (7.8 x DIA 6.5 in)	290 x DIA 265 mm (11.4 x DIA 10.4 in)	—
Maximum Dimensions Trunnion-mounted shaker	—	120 x 117 x 100 mm (4.7 x 4.6 x 3.9 in)	274 x 259 x 165 mm (10.8 x 10.2 x 6.5 in)	395 x 375 x 275 mm (15.6 x 14.8 x 10.8 in)	—

* Half-sine shock force is calculated with the standard payload, 2 ms pulsewidth, 10% pre/post pulse.

† Displacement can vary with payload and shaker orientation. Please contact Brüel & Kjær for advice on specific test requirements.

‡ Measured at a distance of 1 m (3.3 ft) and at a height of 1.6 m (5.2 ft) above floor level in an enclosed cell.

Linear Power Amplifiers



left to right: LPA100 Amplifier, LPA600 Amplifier, LPA1000 Amplifier

Features

- Multi-function display
- Electronic peak current limiting
- Continuously variable gain control with integral reset
- Continuously variable current limit control

The LDS® LPA100 Linear Power Amplifier has been designed primarily to drive the LDS V100 Series and V200 Series shakers.

The LDS LPA600 Linear Power Amplifier has been designed primarily to drive the LDS V400 Series, and V450 Series shakers.

The LDS LPA1000 Linear Power Amplifier has been designed to work with the larger V455 Series permanent magnet shakers.

LDS Linear Power Amplifier Model	LPA100	LPA600	LPA1000
Classification	class B linear amplifier, air-cooled		
Input Supply (±10%)	100, 120, 230 V, at 50/60 Hz		
Input kVA	<0.44 kVA	<1.85 kVA	<2.70 kVA
Rated Power Output	94 W in 3.15 Ω	656 W in 2.5 Ω	961 W in 4.0 Ω
Maximum Power Output Capacity	154 VA in 3.15 Ω	810 VA in 2.5 Ω	1296 VA in 4.0 Ω
Gain	22 V/V ± 2 dB max.	45 V/V ± 2 dB max.	72 V/V ± 2 dB max.
Monitoring Output — Voltage	0.1V/V ± 3%, 5 Hz to 15 kHz	0.05V/V ± 3%, 5 Hz to 10 kHz	0.05V/V ± 3%, 5 Hz to 10 kHz
Monitoring Output — Current	0.1V/A ± 3%, 5 Hz to 15 kHz	0.1V/A ± 3%, 5 Hz to 10 kHz	0.1V/A ± 3%, 5 Hz to 10 kHz
Frequency Range at Maximum Power	dc to 15 kHz for 30 mins at max. VA	40 Hz to 10 kHz for 30 mins at max. VA	
Total Harmonic Distortion at Rated Output	<0.1%, 15 Hz to 5 kHz <0.2%, 5 kHz to 15 kHz	<0.2%, 40 Hz to 5 kHz <0.3%, 5 kHz to 10 kHz	
Maximum Output Voltage — no load	22 Vrms, dc to 15 kHz	45 Vrms, dc to 10 kHz	72 Vrms, dc to 10 kHz
Output Current at Rated VA	5.5 A rms	16.2 A rms	15.5 A rms
Maximum Output Current	7.0 A rms, dc to 15 kHz for 30 mins	17.75 A rms, 40 Hz to 10 kHz for 30 mins	
Signal-to-Noise Ratio	> 95 dB		
Amplifier Efficiency	52 %	57 %	64 %
Sound Power Level at 2m (6.6 ft)	41 dBA	45 dBA	49 dBA
Max. Ambient Working Temperature	35 °C (95 °F)		
Weight	14.0 kg (31 lb)	26.8 kg (59 lb)	33.5 kg (73.9 lb)
Height	88 mm (3.5 in) excluding feet	132 mm (5.2 in) excluding feet	
Width	482.6 mm (19.0 in), with flanges for standard 19" rack mounting		
Depth	450 mm (17.7 in)	450 mm (17.7 in)	550 mm (21.6 in)

SM34205D		
Continuous Torque	7.91	in-lb
	126	oz-in
	0.89	N-m
Peak Torque	24.91	in-lb
	399	oz-in
	2.81	N-m
Nominal Continuous Power	324	Watt
No Load Speed	4,500	RPM
Max. Continuous Current* @ 3750 RPM	8.28	Amps
Peak Power @ 2250 RPM	455	Watts
Voltage Constant	10.8	V/kRPM
Inductance	0.596	mH
Encoder Resolution	8,000	Counts/Rev
Rotor Inertia	0.012	oz-in-sec ²
	8.448	10 ⁻⁴ Kg-m ²
Weight	3.5	lb
	1.59	kg
Shaft Diameter	0.375	in
	9.53	mm
Shaft, Radial Load	15	lb
	6.80	kg
Shaft, Axial Thrust Load	3	lb
	1.36	kg
DeviceNet Available	Yes	
PROFIBUS Available	Yes	
CANopen Available	Yes	

*Default voltage is 48V. See graphs for additional voltages.

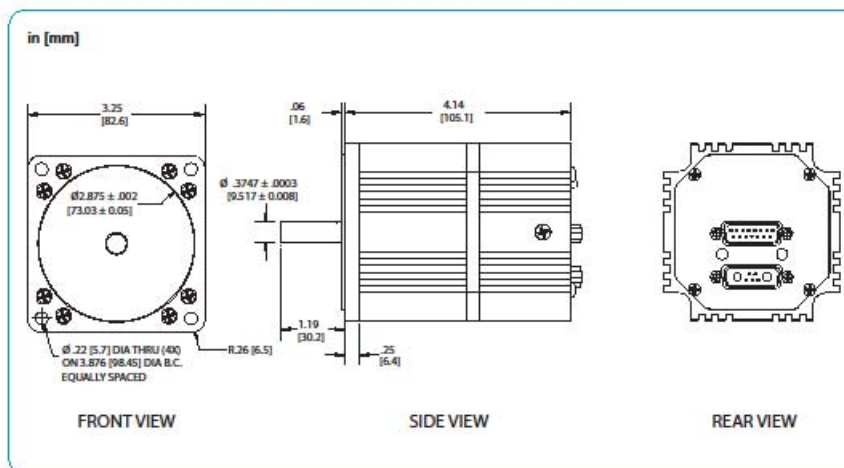


Operating temperature range: 0°C–85°C
Storage temperature range: -10°C–85°C, noncondensing

NOTE: Motor specifications are subject to changes without notice. Consult website and factory for latest data.



Moog Animatics SmartMotor SM34205D (No Options) CAD Drawing



Moog Animatics • www.animatics.com

[sonicjapan.com\)](#)[ansonicasia.com/?](#)

31a2d6f09be657b8e4115a77be9926f.1539826450365.1539826450365.1539830368305.2&__hssc=18166054.4.1539830368305&__hsfp=3406524498)

[Home \(/\)](#)[Products \(/products/\)](#)[Applications \(/applications/\)](#)[Studies \(/studies/\)](#)[Resources \(/resources/\)](#)[About Us \(/about-us/\)](#)

T402/T403 Multi-Channel Research Consoles

Modular Research Consoles for Ultimate Flexibility

Mix and match measurement capabilities in a single instrumentation console. T402 and T403 Consoles are multi-channel capacity cases with a shared universal power supply and back-panel analog outputs compatible with most data acquisition systems. The Consoles accept any 400-Series Module:

- TS410 Tubing Flow Module
- TS420 Perivascular Flow Module

◦ T402

T402 Console holds up to 2 double-bay flow modules, 4 single-bay pressure modules or a combination of both.

◦ T403

T403 Console holds up to 3 double-bay flow modules, 6 single-bay pressure modules or a combination of both.



[Contact us for availability \(/contact-us\)](#)

Product Info

[Product Overview](#)[Related Products](#)[Documents \(2\)](#)

Product Overview

Applications

[Bioprocess](#)[\(/applications/bioprocess\)](#)[Cardiovascular](#)[\(/applications/research/cardiovascular\)](#)[Neurophysiology](#)[\(/applications/research/neurophysiology\)](#)[Pharmacology](#)[\(/applications/research/pharmacology\)](#)[Tubing Model Applications](#)[\(/applications/research/tubing-\)](#)

Each Console may be ordered individually or with any number & combination of Modules. T400-Series Consoles are not standalone units; at least one Module is required to take measurements.

Not for use in humans.

Specifications

T402/T403 Consoles are not standalone units and must be used with a 400-Series Module. Accuracy specifications are linked to the specific Flowprobe or Flowsensor, and represent entire system specifications.

model-applications)

Translational Research
(/applications/research/translational-research)

 Manual

 Request Info

Related Products



(/product/ts420-flow-module/)
TS420 Perivascular Flow Module
(/product/ts420-flow-module/)



(/product/confidence-flowprobes-for-research/)
CO Confidence Flowprobes for Research (PAU-Series)
(/product/confidence-flowprobes-for-research/)



(/product/nanoprobes-ps-series/)
Nanoprobes (PS-Series)
(/product/nanoprobes-ps-series/)



(/product/nanoprobes-v-series/)
Nanoprobes (V-Series)
(/product/nanoprobes-v-series/)



(/product/ps-series-flowprobes/)
PS-Series Flowprobes
(/product/ps-series-flowprobes/)



(/product/pr-series-flowprobes/)
PR-Series Flowprobes
(/product/pr-series-flowprobes/)



(/product/pmp-handle-flowprobes/)
PMP Handle Flowprobes
(/product/pmp-handle-flowprobes/)



(/product/ts410-tubing-module/)
TS410 Tubing Module
(/product/ts410-tubing-module/)




(/product/pxl-clamp-on-flowsensor/)
PXL Clamp-On Flowsensor
(/product/pxl-clamp-on-flowsensor/)




(/product/pxn-inline-flow-sensors/)
PXN Inline Flow Sensors
(/product/pxn-inline-flow-sensors/)

Support Documents

[View All Resources \(/resources\)](/resources/)

 Pub Brief (Kassimis 2018) False Positive Transit Time Flowmetry Graft Failure in Multivessel Coronary Spasm following Off-Pump Coronary Artery Bypass Grafting, Case Rep (</resources/cardiothoracic/pub-brief-kassimis-2018-false-positive-transit-time-flowmetry-graft-failure-in-multivessel-coronary-spasm-following-off-pump-coronary-artery-bypass-grafting-case-rep/>) (A4 Version (</index.cfm/tasks/render/file/?fileID=B8B27027-2A68-4B34-A2E07CCE73B05720>))

 ELSA Delivered Blood Flow and Cardiac Output (</resources/extracorporeal-ecmo-cp-bypass/elsa-delivered-blood-flow-and-cardiac-output/>) (A4 Version (</tasks/render/file/?fileID=B4F5FA68-1310-4CFE-B9994EE7AAEE2A03>))

[News \(/about-us/news/\)](/about-us/news/) [Events \(/about-us/events/\)](/about-us/events/)

[Software Updates \(/software-updates/\)](/software-updates/) [Contact \(/contact-us/\)](/contact-us/)

[Privacy Policy \(/about-us/privacy-policy/\)](/about-us/privacy-policy/)

[Partner Portal \(/partner-portal/\)](/partner-portal/)



PRODUCT OVERVIEW

Dragon Skin® silicones are high performance platinum cure liquid silicone compounds that are used for a variety of applications ranging from creating skin effects and other movie special effects to making production molds for casting a variety of materials. Because of the superior physical properties and flexibility of Dragon Skin® rubbers, they are also used for medical prosthetics and customizing applications. Dragon Skin® rubbers are also used for a variety of industrial applications and have a service temperature range of a constant -70°F to +400°F (-21°C to +205°C).

Great for Making Molds for a Variety of Applications - Available in Shore 10A, 20A and 30A. Dragon Skin® silicones can be used to make exceptionally strong and tear resistant molds for casting plaster, wax, concrete (limited production run), resins and other materials.

Time Tested, Versatile Special Effects Material - Soft, super-strong and stretchy, Dragon Skin® 10 (Very Fast, Fast, Medium and Slow speeds) is used around the world to make spectacular skin and creature effects. An infinite number of color effects can be achieved by adding Sic Pig® silicone pigments or Cast Magic® effects powders. Cured rubber can also be painted with the Psycho Paint® system. Cured material is skin safe and certified by an independent laboratory to ISO 10993-10. Biological evaluation of medical devices. Part 10: Tests for irritation and skin sensitization.

Easy To Use - Dragon Skin® silicones are mixed 1A:1B by weight or volume. Liquid rubber can be thinned with Silicone Thinner® or thickened with TH-VEY®. Rubber cures at room temperature (73°F/23°C) with negligible shrinkage. Vacuum degassing is recommended to minimize air bubbles in cured rubber.

TECHNICAL OVERVIEW

	Mixed Viscosity (ASTM D-2393)	Specific Gravity (g/cc) (ASTM D-1435)	Specific Volume (cc) (ASTM D-1435)	Pot Life (ASTM D-2471)	Cure Time	Shore A Hardness (ASTM D-2240)	Tensile Strength (ASTM D-412)	100% Modulus (ASTM D-412)	Elongation at Break % (ASTM D-412)	Die B Tear Strength (ASTM D-624)	Shrinkage (in./in.) (ASTM D-2566)
Dragon Skin® 10 Very Fast	23,000 cps	1.07	25.8	4 min.	30 min.	10A	475 psi	22 psi	1000%	102 pli	< .001 in./in.
Dragon Skin® 10 Fast	23,000 cps	1.07	25.8	8 min.	75 min.	10A	475 psi	22 psi	1000%	102 pli	< .001 in./in.
Dragon Skin® 10 Medium	23,000 cps	1.07	25.8	20 min.	5 hours	10A	475 psi	22 psi	1000%	102 pli	< .001 in./in.
Dragon Skin® 10 Slow	23,000 cps	1.07	25.8	45 min.	7 hours	10A	475 psi	22 psi	1000%	102 pli	< .001 in./in.
Dragon Skin® 20	20,000 cps	1.08	25.6	25 min.	4 hours	20A	550 psi	49 psi	620%	120 pli	< .001 in./in.
Dragon Skin® 30	30,000 cps	1.08	25.7	45 min.	16 hours	30A	500 psi	86 psi	364%	108 pli	< .001 in./in.

Mix Ratio: 1A:1B by volume or weight
Color: Translucent

Useful Temperature Range: 65°F to +450°F (-53°C to +232°C)
Dielectric Strength (ASTM D-14-92a): >350 volts/mil

*All values measured after 7 days at 73°F/23°C

PROCESSING RECOMMENDATIONS

PREPARATION... Safety - Use in a properly ventilated area ("room size" ventilation). Wear safety glasses, long sleeves and rubber gloves to minimize contamination risk. Wear vinyl gloves only. Latex gloves will inhibit the cure of the rubber.

Store and use material at room temperature (73°F/23°C). Warmer temperatures will drastically reduce working time and cure time. Storing material at warmer temperatures will also reduce the usable shelf life of unused material. These products have a limited shelf life and should be used as soon as possible.

Cure Inhibition - Addition-cure silicone rubber may be inhibited by certain contaminants in or on the pattern to be molded resulting in tackiness at the pattern interface or a total lack of cure throughout the mold. Latex, tin-cure silicone, sulfur clays, certain wood surfaces, newly cast polyester, epoxy, tin cure silicone rubber or urethane rubber may cause inhibition. If compatibility between the rubber and the surface is a concern, a small-scale test is recommended. Apply a small amount of rubber onto a non-critical area of the pattern. Inhibition has occurred if the rubber is gummy or uncured after the recommended cure time has passed.

Because no two applications are quite the same, a small test application to determine suitability for your project is recommended if performance of this material is in question.

Safety First!

The Material Safety Data Sheet (MSDS) for this or any Smooth-On® product should be read prior to use and is available upon request from Smooth-On. All Smooth-On products are safe to use if directions are read and followed carefully.

Keep Out of Reach of Children

Be careful. Use only with adequate ventilation. Contact with skin and eyes may cause irritation. Flush eyes with water for 15 minutes and seek immediate medical attention. Remove from skin with waterless hand cleaner followed by soap and water.

Important: The information contained in this bulletin is considered accurate. However, no warranty is expressed or implied regarding the accuracy of the data. The results to be obtained from the use thereof or that any such use will not infringe upon a patent. User shall determine the suitability of the product for the intended application and assume all risk and liability whatsoever in connection therewith.

Cure Inhibition - To prevent inhibition, one or more coatings of a clear acrylic lacquer applied to the mold surface is usually effective. Allow any sealer to thoroughly dry before applying rubber. Note: Even with a sealer, platinum silicones will not work with modeling clays containing heavy amounts of sulfur. Do a small scale test for compatibility before using on your project.

Applying A Release Agent - Although not usually necessary, a release agent will make demolding easier when pouring into or over most surfaces. Ease Release® 200 is a proven release agent for making molds with silicone rubber. Mann Ease Release® products are available from Smooth-On or your Smooth-On distributor.

IMPORTANT: To ensure thorough coverage, lightly brush the release agent with a soft brush over all surfaces of the model. Follow with a light mist coating and let the release agent dry for 30 minutes.

If there is any question about the effectiveness of a sealer/release agent combination, a small-scale test should be made on an identical surface for trial.

MEASURING & MIXING...

Before you begin, pre-mix Part B thoroughly. After dispensing required amounts of Parts A and B into mixing container (1A:1B by volume or weight), mix thoroughly for 3 minutes making sure that you scrape the sides and bottom of the mixing container several times. After mixing parts A and B, vacuum degassing is recommended to eliminate any entrapped air. Vacuum material for 2-3 minutes (29 inches of mercury), making sure that you leave enough room in container for product volume expansion.

POURING, CURING & MOLD PERFORMANCE...

For best results, pour your mixture in a single spot at the lowest point of the containment field. Let the rubber seek its level up and over the model. A uniform flow will help minimize entrapped air. The liquid rubber should level off at least 1/2" (1.3 cm) over the highest point of the model surface.

Curing / Post Curing - Allow rubber to cure as prescribed at room temperature (73°F/23°C) before demolding. Do not cure rubber where temperature is less than 65°F/18°C. **Optional:** Post curing the mold will aid in quickly attaining maximum physical and performance properties. After curing at room temperature, expose the rubber to 776°F/80°C for 2 hours and 212°F/100°C for one hour. Allow mold to cool to room temperature before using.

If Using As A Mold - When first cast, silicone rubber molds exhibit natural release characteristics. Depending on what is being cast into the mold, mold lubricity may be depleted over time and parts will begin to stick. No release agent is necessary when casting wax or gypsum. Applying a release agent such as Ease Release® 200 (available from Smooth-On) prior to casting polyurethane, polyester and epoxy resins is recommended to prevent mold degradation.

Thickening Dragon Skin® Silicones - TH-VEY® is made especially for thickening Smooth-On's silicones for vertical surface application (making brush-on molds). Different viscosities can be attained by varying the amount of TH-VEY®. See the TH-VEY® technical bulletin (available from Smooth-On or your Smooth-On distributor) for full details.

Thinning Dragon Skin® Silicones - Smooth-On's Silicone Thinner® will lower the viscosity of Dragon Skin® for easier pouring and vacuum degassing. A disadvantage is that ultimate tear and tensile are reduced in proportion to the amount of Silicone Thinner® added. It is not recommended to exceed 10% by weight of total system (A+B). See the Silicone Thinner® technical bulletin (available from Smooth-On or your Smooth-On distributor) for full details.

Mold Performance & Storage - The physical life of the mold depends on how you use it (materials cast, frequency, etc.). Casting abrasive materials such as concrete can quickly erode mold detail, while casting non-abrasive materials (wax) will not affect mold detail. Before storing, the mold should be cleaned with a soap solution and wiped fully dry. Two part (or more) molds should be assembled. Molds should be stored on a level surface in a cool, dry environment.



Call Us Anytime With Questions About Your Application.

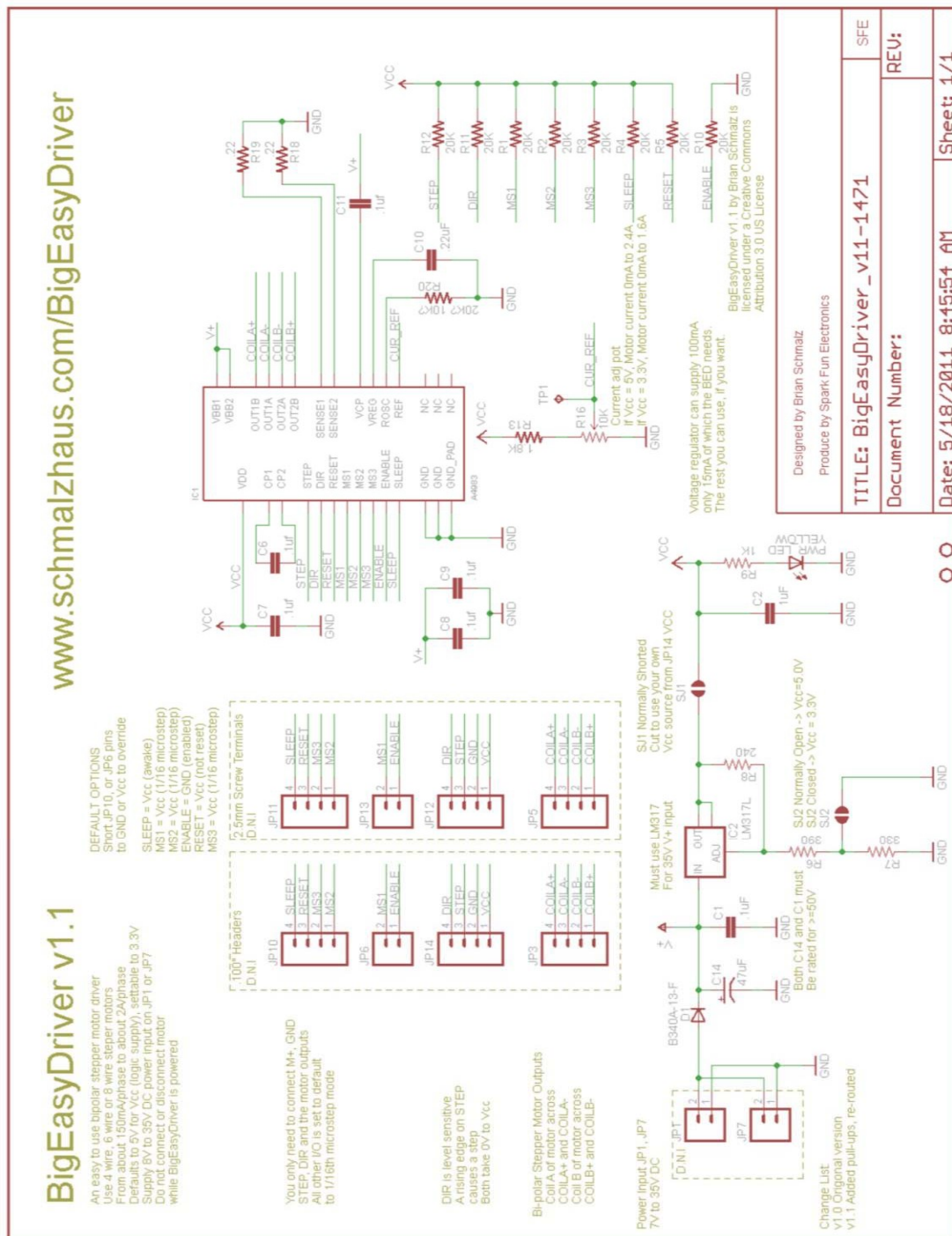
Toll-free: (800) 381-1733 Fax: (610) 252-6200

The new www.smooth-on.com is loaded with information about mold making, casting and more.

072516-R

Appendix E: Easy Driver Schematic

V1.1



References

1. “Circulatory System,” Pinterest. [Online]. Available: <https://www.pinterest.nz/ArtInBiology/circulatory-system/>. [Accessed: 16-Jul- 2018].
2. Hall, J.E (2011). *A textbook of medical physiology*, 13e. Elsevier, Philadelphia, USA
3. Marieb, E.N (2014). *Essentials of Human Anatomy and Physiology*: Pearson Education Ltd. London, UK, Page 400-403.
4. Fiore, M. S. H. Schmidt, I. G. (1974). *Atlas of human histology*: Lea & Febiger, Philadelphia,
5. Lang, E. V. (1997). *Functional Abnormalities of the Aorta*. Journal of Vascular and Interventional Radiology, Vol. 3, Issue 8, pp. 382.
6. Nichols, W., O'Rourke, M., & Vlachopoulos, C. (2011). *McDonald's blood flow in arteries: Theoretical, experimental and clinical principles*: CRC Press.
7. “CV Physiology: Arterial Blood Pressure.” [Online]. Available: <https://www.cvphysiology.com/Blood%20Pressure/BP001>. [Accessed: 15- Jul -2018].
8. El Baroudi, F. Razafimahery, N. Bideau and L. Rakotomanana, “ *Influence of the fluid-structure interaction in biomechanics: application to parametric modal analysis and dynamics of the aorta under a shock*”, Int. J. Biomedical Engineering and Technology, Vol. 5, Issue 2-3, p 103, 2011.
9. M. Hanss, J. Herrmann, T. Haag, “*Vibration Analysis of Fluid-Filled Piping Systems with Epistemic Uncertainties*”, UTAM Symposium on the Vibration Analysis of Structures with Uncertainties, IUTAM Book series Vol. 27, pp 43-56, 2011.
10. A. Mattheisa, M. Trobitza, K. Kussmaulb, K. Kerkhofb, “*Diagnostics of piping by ambient vibration analysis*”, Nuclear Engineering and Design, Vol. 198, Issues 1–2, pp 131–140, 2000.
11. P. V. Feodos’ev, “*Vibrations and Stability of a Pipe When Liquid Flows Through It*”, Inzhenernyi Sbornik, Vol. 10, pp. 169–170, 1951.
12. M. A. Langthjem, “*Finite Element Analysis and Optimization of a Fluid-Conveying Pipe*”, Mech.Struct.Mach., Vol. 23, pp. 343–376, 1995.
13. M. Yoshizawa, K. Ueno, E. Hasegawa, Y. Tsujioka, “*Lateral Vibration of a Cantilevered Flexible Pipe Conveying Fluid A Horizontal Excitation at the Upper End of the vertical pipe*”, Trans. Jpn. Soc. Mech. Eng., Ser. C, Vol. 54, pp. 100–107, 1988.
14. W. H. Miles, C. Pezeshki, S. Elgar, “*Bispectral Analysis of a Fluid Elastic System: The Cantilevered Pipe*”, J. Fluids Structures, Vol. 6, pp. 633– 640, 1992.
15. J. S. Jensen, “*Fluid Transport Due to Nonlinear Fluid-Structure Interaction*”, J. Fluids Struct. Vol. 11, pp. 327–344, 1997.

16. M. Yoshizawa, H. Ogino, E. Hasegawa, "*Lateral Vibration of a Cantilevered Pipe Conveying Fluid at Finite Amplitude*", Proceedings of the ASME Winter Annual Meeting, Applied Mechanics Division, AMD, Stability and Control of Pipes Conveying Fluid, Anaheim, CA, Vol. 152, pp. 11–24, 1992.
17. M. J. Hannoyer, M. P. Païdoussis, "*Instabilities of Tubular Beam Simultaneously Subjected to Internal and External Axial Flows*", ASME J. Mech. Design, Vol. 100, Issue 2, pp. 328–336, 1978.
18. S. U. Siddiqui, M. K. Verma, S. Mishra, S. Gupta, "*Mathematical modelling of pulsatile flow of Casson's fluid in arterial stenosis*", J. Applied Mathematics and Computation, Vol. 210, pp.1-10, 2009.
19. C. Tu, M. Deville, "*Pulsatile flow of non-Newtonian fluids through arterial stenosis*", J. Biomechanics, Vol. 29, Issue 7, pp.899-908, 1996.
20. R. Budwig, D. Elger, H. Hooper, J. Slippy, "*Steady flow in abdominal Aortic aneurysm models*", ASME J. Biomech. Eng., Vol. 115, pp.419–423, 1993.
21. M. W. Lesmez,(1989). *Modal analysis of vibrations in liquid-filled piping systems*, Michigan State University, ProQuest, UMI Dissertations Publishing.
22. El Baroudi, F. Razafimahery, L. R. Rakotomanana, "*Dynamics of the aortic arch submitted to a shock loading: Parametric study with fluid-structure models*", International Journal for Numerical Methods in Biomedical Engineering, Vol. 28, Issue 1, pp. 100-110, 2012.
23. A. M. Al-Jumaily, P. Mbikou, P. R. Redey, "*Effect of length oscillations on airway smooth muscle reactivity and cross-bridge cycling*", American Journal of Physiology-Lung Cellular and Molecular Physiology, Vol. 303, Issue 4, p. 286-294, 2012.
24. Y. Du, A. M. Al-Jumaily, H. Shukla, "*Smooth muscle stiffness variation due to external longitudinal oscillations*", Journal of Biomechanics, Vol. 40 Issue 14, pp.3207–3214, 2007.
25. G. Ijpma, A. M. Al-Jumaily, S. P. Cairns, G. C. Sieck, "*Logarithmic superposition of force response with rapid length changes in relaxed porcine airway smooth muscle*", American Journal of Physiology-Lung Cellular and Molecular Physiology, Vol. 299, Issue 6, L898–L904, 2010.
26. N. Westerhof, B. Westerhof, "*A review of methods to determine the functional arterial parameters stiffness and resistance*", Journal of Hypertension, Wolters Kluwer Health Lippincott Williams & Wilkins, Vol. 31, pp1765-1775, 2013.

27. J. Alastruey, K. H. Parker, J. Peiró, S. J. Sherwin, “*Analysing the pattern of pulse waves in arterial networks: a time domain study*”, Journal of Engineering Math., Vol. 64, pp. 331–351, 2009
28. S. J. Sherwin¹, L. Formaggia, J. Peiro and V. Franke, “*Computational modelling of 1D blood flow with variable mechanical properties and its application to the simulation of wave propagation in the human arterial system*”, Int. J. Numerical Methods Fluids, Vol. 43, pp. 673–700, 2003
29. A. Anssari-Benam and T. Korakianitis, “*An experimental Model to Simulate Arterial Pulsatile Flow: In Vitro Pressure and Pressure Gradient Wave Study*”, Society for Experimental Mechanics Vol. 53, pp. 649–660, 2003
30. D.N. Ku, “*Blood flow in arteries*”, Ann Rev Fluid Mech (1997) 29:399–434
31. M.X. Li, J.J. Beech-Brandta, L.R. John, P.R. Hoskins, W.J. Easson, “*Numerical analysis of pulsating blood flow and vessel wall mechanics in different of stenosis*”, J Biomechanics, Vol. 40, pp. 715-3724, 2007
32. B.E. Westerhof, I. Guelen, W.J. Stok, K.H. Wesseling, J.A.E. Spaan, N. Westerhof, W.J.Bos and N. Stergiopulos, “*The quantitative contribution of all local conduit arterial, blood, and distal load properties to the pressure transfer function from brachial artery to aorta*”, American Journal of Physiological Heart Circ Physiol., Vol. 292, H800 –H807, 2007.
33. D.A. Johnson, U.P. Naik, and A.N. Beris, “*Efficient implementation of the proper outlet flow conditions in blood flow simulations through asymmetric arterial bifurcations*”, Int. J. Numer. Meth. Fluids, Vol. 66, pp. 1383–1408, 2011
34. B.E. Westerhof, I. Guelen, N. Westerhof, J.M. Karemaker, A. Avolio, “*Quantification of wave reflection in the human aorta from pressure alone – a proof of principle*”, Hypertension, Vol. 48, pp. 595– 601, 2006
35. A. Qasem and A. Avolio, “*Determination of aortic pulse wave velocity from waveform decomposition of the central aortic pressure pulse*”, Hypertension, Vol. 51, pp.188 – 195, 2008
36. J.G. Kips, E.R. Rietzschel, M.L. De Buyzere, B.E. Westerhof, T.C. Gillebert, L.M. Van Bortel, P. Segers, “*Evaluation of Non-invasive Methods to Assess Wave Reflection and Pulse Transit Time From the Pressure Waveform Alone*”, Hypertension, Vol. 53, pp. 142-149, 2009

37. T. Anor, L. Grinberg, H. Baek, J.R. Madsen, M.V. Jayaraman, and G. E. Karniadakis, “*Modelling of blood flow in arterial trees*”, John Wiley & Sons, Inc. WIREs Syst Biol Med., Vol. 2, pp. 612-623, 2010
38. E.O. Oghre and C.E. Omole, “*Comparison of One-Dimensional and Two-Dimensional Arterial Models*”, Journal of Applied sciences 6(14): 2932-2935, 2006
39. P.Crosetto, P. Reymond, S.Deparis, D. Kontaxakis, N. Stergiopulos, A. Quarteroni, “*Fluid-structure interaction simulation of aortic blood flow*”, Computers & Fluids, Elsevier, j.compfluid., Vol. 43, pp. 46-47, 2010
40. C.S. Park, S.J. Payne, “*Nonlinear and viscous effects on wave propagation in an elastic axisymmetric vessel*”, Elsevier J of Fluid and Structures, Vol. 27, pp. 134-144, 2010
41. A.P. Avolio, “*Multibranched model of the human arterial system*”, Med.Biol.Eng.Comput., Vol. 18, pp. 709-718, 1980
42. M. Karamanoglu, D. Gallaghe, A.P. Avolio and M.F. O'Rourke, “*Functional origin of reflected pressure waves in a multibranched model of the human arterial system*”, The American Physiological Society, Vol. 94, pp. 0363-6135, 1994
43. W.W. Nichols, D.G. Edwards, “*Arterial Elastance and Wave Reflection Augmentation of Systolic Blood Pressure: Deleterious Effects and Implications for Therapy*”, J Cardiovasc. Pharmacol. Therapeutics, Vol. 6, Issue 1, pp. 5-21, 2001
44. Fung, Y.C (1993). *Biomechanics: mechanical properties of living tissues*, 2e, New York: Springer.
45. G.S. Kassab, “*Biomechanics of the cardiovascular system: the aorta as an illustrative example*”, J. R. Soc. Interface, Vol. 3, pp. 719-740, 2006
46. K.S. Matthysa, J. Alastrueya, J. Peiro, A.W. Khir, P. Segersd, P.R. Verdonck, K.H. Parker, S.J. Sherwin, “*Pulse wave propagation in a model human arterial network: Assessment of 1-D numerical simulations against in vitro measurements*”, Journal of Biomechanics, Vol. 40, pp. 3416-3486, 2007
47. F.N. van de Vosse, and N. Stergiopulos, “*Pulse Wave Propagation in the Arterial Tree*”, Annu. Rev. Fluid Mechanics, Vol. 43, pp. 467–99, 2011
48. E.G.H.J. Martens, L.L.H. Peeters, E.D. Gommer, W.H. Mess, F.N. van de Vosse, et al. “*The visually-evoked cerebral blood flow response in women with a recent history of preeclampsia and/or eclampsia*”, Ultrasound Med. Biol., Vol. 35, pp.1–74, 2009
49. Chaudhry, M.H. (1987). *Applied hydraulic transients*: Van Nostrand Reinhold, New York.

50. A.S Elansary, W. Silva, M.H. Chaudhry, “ *Numerical and experimental investigation of transient pipe flow*”, J. Hydraulic Res., Vol. 32, Issue 5, pp. 689–706, 1994
51. H.. Reddy, M.H. Chaudhry and P.K. Mohapatra, “ *Modelling of periodic flows in pipelines by transfer function method*”, Journal of Hydraulic Research, Vol. 48, Issue 2, pp. 255-259, 2010
52. S. Ajgaonkar (2017). *Effect of Vibration imposition on Aortic Muscle Tissue: An explorative study*. School of Interprofessional Health studies and School of Engineering, AUT, Auckland.
53. C. Russ, M. Gessat, V. Falk, and G. Székely, “*Rapid prototyping of silicone-based phantom models for stent simulation validation,*” Proc. MICCAI-Stent, vol. 12, 2012.
54. G. V. Savrasov, A. F. Batanov, and S. G. Gusarov, “*A Model of the Human Arterial System,*” Biomed. Eng., vol. 45, no. 3, pp. 77–81, 2011.
55. M. Johnson, “*Creating a synthetic aorta for the means to study arterial pulse wave velocity,*” N/A, Jun. 2016.
56. P.N.W. Jones (2017). *Developing a novel extra-aortic cuff with peristaltic motion and counterpulsation to assist heart function*: School of Engineering, Faculty of Design and Creative Technologies, AUT, Auckland
57. Wolfram (2017). “Mathematica[®]10”, Wolfram Research of Champaign, Illinois, USA.
58. Smooth-on (2017). *Dragon Skin[®]10*. [Online]. Available: <https://www.smooth-on.com/products/dragon-skin-10-medium/> [Accessed]: [15-Jul- 2018]